A Diversity of Metal–Ligand Interactions in Halide (X = I, Br, Cl, F) and Halide-Free Ambiphilic Ligand Rhodium Complexes

Bradley E. Cowie, David J. H. Emslie, Hilary A. Jenkins,[†] and James F. Britten[†]*

Department of Chemistry and Chemical Biology, McMaster University, 1280 Main Street West, Hamilton, ON, L8S 4M1, Canada.

[†] McMaster Analytical X-Ray Diffraction Facility

RECEIVED DATE (to be automatically inserted after your manuscript is accepted if required according to the journal that you are submitting your paper to)

*To whom correspondence should be addressed.

Phone: 905-525-9140, Fax: 905-522-2509. E-mail: emslied@mcmaster.ca.

Abstract:

Reaction of the neutral ambiphilic ligand 2,7-di-*tert*-butyl-5-diphenylboryl-4-diphenylphosphino-9,9-dimethylthioxanthene (TXPB) with [{Rh(μ-Cl)$(CO)_2$}$_2$] yields [RhCl(CO)(TXPB)] (**1**) (Emslie *et al. Organometallics*, **2006**, *25*, 5835). Complex **1** is square planar with the TXPB ligand bound to rhodium via the phosphine and thioether donors (these are features common to complexes **2–5**, *vide infra*). Treatment of **1** with Me_3SiBr and Me_3SiI allowed for halide substitution to afford [RhBr(CO)(TXPB)] (**2**) and [RhI(CO)(TXPB)] (**3**), respectively. The halide co-ligands in complexes **1** and **2** form a strong bridging interaction between rhodium and the borane group in TXPB. The presence of stronger borane–halide coordination in **1** is clearly illustrated by an ^{11}B NMR chemical shift of 12 ppm versus 27 ppm in **2**. In contrast, the iodide ligand in **3** forms only a weak bridging interaction to boron, leading to a B···I distance of 3.125(7) Å, and an ^{11}B NMR chemical shift of 56 ppm (*versus* 69 ppm for free TXPB). A lower carbonyl stretching frequency in **3** (2002 cm^{-1}) versus **1** or **2** (2008 and 2013 cm^{-1}, respectively) could be attributed to weakening of the Rh–X bond in **1** and **2** as a consequence of halide–borane coordination and/or a shorter Rh–S bond in complex **3**. [Rh(CO)(TXPB–F)] (**4**) and the halide-free cation [Rh(CO)(TXPB)][PF_6] (**5**) were accessed by reaction of **1** with [NMe_4]F and Tl[PF_6], respectively. Complex **4** is zwitterionic with fluoride bound to boron [^{11}B NMR δ 4 ppm; B–F = 1.445(6) Å; Rh···F = 3.261(3) Å] and an η^2-interaction between the cationic rhodium centre and the *ipso*- and *ortho*-carbon atoms of a *B*-aryl ring in TXPB–F. By contrast, rhodium in **5** engages in an η^2-interaction with boron and the *ipso*-carbon of one *B*-phenyl ring; Rh–B and Rh–C_{ipso} bond lengths in **5** are 2.557(3) and 2.362(2) Å, respectively. The long Rh–B distance and an ^{11}B NMR chemical shift of 57 ppm are consistent with only a weak Rh–B interaction in **5**, and a CO stretching frequency of 2028 cm^{-1} (Nujol), *versus* 2004–2013 cm^{-1} for complexes **1–4**, is indicative of greatly reduced electron density in **5**, relative to **1–4**.

Introduction:

The chemistry of ambiphilic borane-containing ligands has seen a burst of activity over the past 10 years, providing a diverse range of complexes, including those containing direct metal-borane interactions.[1] In this area, our research has focused on 2,7-di-*tert*-butyl-5-diphenylboryl-4-diphenylphosphino-9,9-dimethylthioxanthene (TXPB), a rigid phosphine/thioether/borane ligand,[2] and complexes exhibiting a range of metal-TXPB bonding modes have been prepared (Figure 1).[2-4] Metal–chloride–borane bridging interactions such as those in [RhCl(CO)(TXPB)] (**1**),[4] [{PdCl(TXPB)}$_2$] and [PdCl$_2$(TXPB)][3] (D in Figure 1) are rare, and most other examples have been reported by Bourissou. These complexes include: [(*p*-cymene)RuCl$_2${NC$_5$H$_4$(CH$_2$BCy$_2$)-*o*}],[5] [(η^3-allyl)PdCl{P^{i}Pr$_2$(C$_6$H$_4$)BCy$_2$-*o*}],[6] [(NBD)RhCl{P^{i}Pr$_2$(C$_6$H$_4$)BCy$_2$-*o*}] (NBD = norbornadiene), [(PdCl$_2${P^{i}Pr$_2$(C$_6$H$_4$)BCy$_2$-*o*})$_2$], and [PdCl$_2$(PPh$_3$){P^{i}Pr$_2$(C$_6$H$_4$)BCy$_2$-*o*}] (Figure 2).[7] Additional complexes containing a metal–chloride–borane interaction are Bochmann's [{η^5-C$_5$H$_4$B(C$_6$F$_5$)$_2$}(L)TiCl$_2$] [L = Cp, C$_5$H$_4$SiMe$_3$, indenyl, and C$_9$H$_6$NMe$_2$ {2-(dimethylamino)indenyl}],[8] Mayer's [(κ^3-Tp)OsCl$_2$(NPhBPh$_2$)],[9] Fontaine's [(IMes)$_2$PtHCl{BC$_5$H$_4$(SiMe$_3$)-*o*}],[10] and Otero's [(η^5-C$_5$H$_4$SiMe$_3$)$_2$(L)NbCl{B(C$_6$F$_5$)$_3$}] (L = CNXyl, CNCy, CO) (Figure 2).[11]

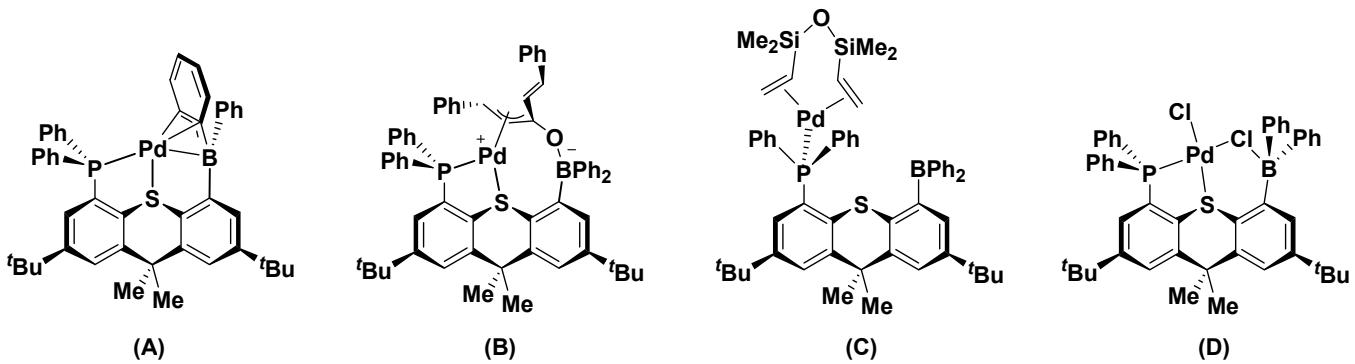

Figure 1. Examples of different metal-TXPB bonding modes: (A) Triarylborane η^3*BCC*-coordination. (B) Zwitterionic boratoxyallyl complex formation induced through binding of an enone co-ligand (dba).

(C) TXPB η^1*P*-coordination induced by metal–diene coordination. (D) Chloride occupying a bridging position between the metal and the borane.

A wide range of complexes in which a fluoroborate anion interacts with a cationic metal centre via a M–F–B bridge have also been prepared (Figure 3).[12] However, complexes containing a metal–bromide–borane or metal–iodide–borane interaction appear to be unknown, presumably due to a decrease in B–X bond energies in the order F > Cl > Br > I. This order was recently demonstrated in the reactivity of a series of late transition metal tris(*N*-*tert*-butylimazolyl)borane complexes; [{κ^4-B(mt$^{t\mathrm{Bu}}$)$_3$}NiCl] reacts with I_2 or $CHBr_3$ to form [{κ^3-ClB(mt$^{t\mathrm{Bu}}$)$_3$}NiX] (X = I or Br) and with XeF_2 to form [{κ^3-FB(mt$^{t\mathrm{Bu}}$)$_3$}NiCl], [{κ^4-B(mt$^{t\mathrm{Bu}}$)$_3$}NiY] (Y = *N*CS or N_3) reacts with I_2 to form [{κ^3-YB(mt$^{t\mathrm{Bu}}$)$_3$}NiI], and [{κ^4-B(mt$^{t\mathrm{Bu}}$)$_3$}Fe(CO)$_2$] reacts with I_2 in $CHCl_3$ to form [{κ^3-ClB(mt$^{t\mathrm{Bu}}$)$_3$}Fe(CO)I].[13] Furthermore, simple boron halides have considerable precedent as reagents for halide metathesis, for example, [{$(Me_2N)(EtO)C$}$AuCl_3$] reacts with BBr_3 to yield [{$(Me_2N)(EtO)C$}$AuBr_3$], which reacts with BI_3 to form [{$(Me_2N)(EtO)C$}AuI_3].[14]

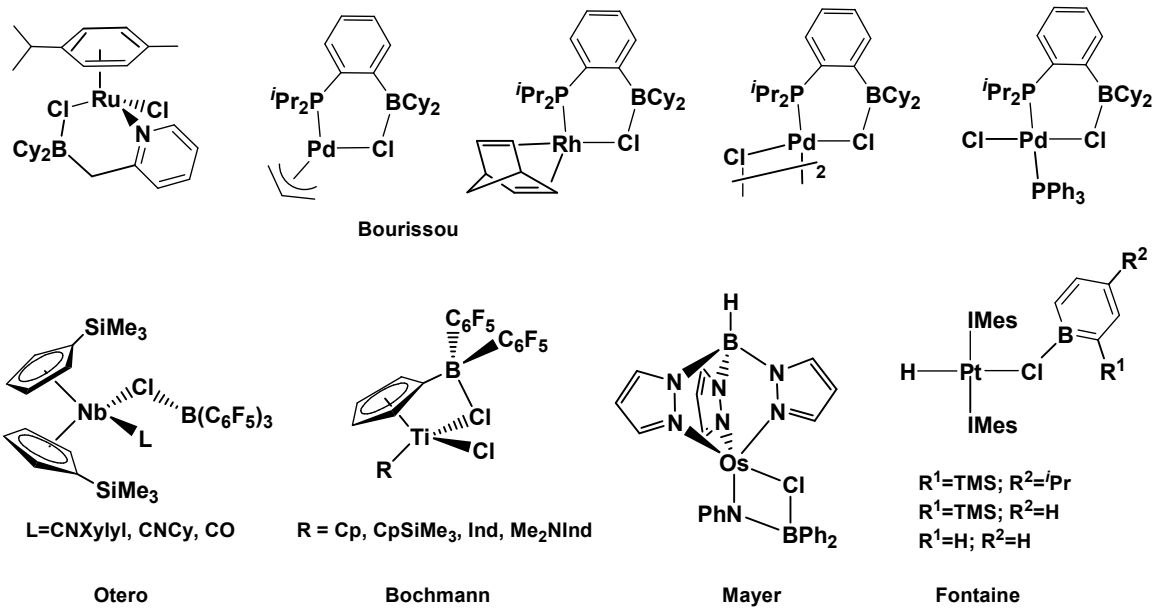

Figure 2. Complexes exhibiting a metal–halide–borane bridging interaction, not including TXPB complexes. Xyl = 2,6-dimethylphenyl; $C_9H_6NMe_2$ = 2-(dimethylamino)indenyl; IMes = 1,3-di(2,4,6-trimethylphenyl)imidazolin-2-ylidene.

An interesting but as yet unrealized possibility for complexes exhibiting metal–halide–borane bridging interactions is their application in C–X bond activation chemistry, for example in C–C bond forming catalysis. A typical cycle for C–C bond formation at palladium (e.g. Suzuki-Miyaura, Stille or Negishi coupling) involves oxidative addition of an aryl halide substrate, followed by transmetallation and reductive elimination. For C–X bond oxidative addition, the order of reactivity is generally Ar–I > Ar–Br > Ar–Cl > Ar–F, consistent with substantial increases in Ar–X bond strength as group 17 is ascended (fluorine forms the strongest of all single bonds to carbon).[15,16] A mismatch between hard fluoride ligands (resulting from Ar–F oxidative addition) and a soft palladium(II) metal centre may also conspire to reduce the thermodynamic driving force for ArF oxidative addition, especially in the absence of strong π-acceptor co-ligands.[16,17] We are interested in exploring the potential for strong M–X–BR_3 interactions to increase the thermodynamic favorability of aryl-chloride and aryl-fluoride oxidative addition, with a view towards eventual applications in C–C bond forming catalysis.[18,19]

Beyond C–X bond activation, ambiphilic ligands offer a more general possibility for cooperative reactivity involving both a metal and a pendant borane. Rare examples of this type of reactivity include: (1) CO insertion reactions at iron or manganese promoted by the pendant alane group of an Ph_2P-N^{t}Bu-AlR_2 (R = Me or Et) ligand,[20] (2) rate enhancements for the dehydrogenative coupling of $PhSiH_3$ by [(Me-Ind)NiMe(PPh_3)] in the presence of $Me_2PCH_2AlMe_2$ (the proposed intermediate in this reactivity is [(Me-Ind)NiMe{$Me_2PCH_2AlMe_2$}], and a related rhodium complex, [Cp*$RhMe_2$(κ^1-$Me_2PCH_2AlMe_2$-OSMe_2)], has also been prepared),[21] and (3) reaction of Na[$H_2B(mt)_2$] with [RhCl(CS)(PPh_3)$_2$] to form [LRhH(PPh_3)] [L = {$H(mt)_2B$}(Ph_3P)C=S], presumably *via* the intermediate [{κ^3-$HB(mt)_2$}RhH(CS)(PPh_3)].[2,22] Reactions of this type rely on the availability of a free pendant group 13 Lewis acid, so we are interested to probe whether like chloride, the heavier halides (bromide and

iodide) engage in metal–halide–bridging. Such interactions would be deleterious to cooperative activation reactivity in ambiphilic ligand complexes, and are of broad significance given the ubiquitous nature of halide ligands in organometallic chemistry.

We report here a series of rhodium(I) halide complexes, [RhX(CO)(TXPB)] (X = Cl, Br, I and F), as well as halide-free [Rh(CO)(TXPB)][PF_6], all of which have been investigated by X-ray crystallography and NMR and IR spectroscopy. [RhX(CO)(TXPB)] complexes were chosen for study in this work, rather than [PdX_2(TXPB)] complexes, for the following reasons: (1) Neutral rhodium(I) complexes contain only one halide co-ligand; in dihalide complexes, halide substitution/abstraction reactions may be complicated by reactivity at different sites, coupled with the presence of only one pendant borane in TXPB to coordinate or abstract a halide from the metal. (2) The products of aryl halide oxidative addition at palladium(0) also contain only one halide ligand. (3) Rhodium-103 is 100% abundant with a nuclear spin of 1/2, so can provide an additional NMR handle to probe the strength of metal–phosphine and/or metal–fluoride interactions. (4) Carbonyl stretching frequencies provide valuable insight into electronic changes occurring at rhodium due to halide substitution or abstraction.

Results and Discussion

A Borane-Bearing Rhodium Chloro Carbonyl Complex. In 2006 we communicated the synthesis of [RhCl(CO)(TXPB)] (**1**) (Scheme 1; Figure 3) as a precursor to [(TXPB)Rh(μ-$CO)_2$Fe(CO)Cp].[4] Complex **1** adopts a distorted square planar geometry [S–Rh–CO = 171.3(3)°; P–Rh–Cl = 172.64(8)°] and contains an uncommon metal-halide-borane bridging interaction. The Rh–Cl bond length of 2.381(2) Å is in good agreement with the Rh–Cl distances in related [RhCl(CO)(PAr_3)(SR_2)][23] complexes, indicating that the Rh–Cl bond is not substantially weakened by triarylborane coordination. However, the B–Cl bond length of 1.995(9) Å does indicate a strong bonding interaction between boron and the bridging chloride, since this distance is only 0.10–0.13 Å longer than that in chloroborate anions[24] and chloroborane Lewis base adducts.[25] The presence of a strong B–Cl interaction in **1** is also supported by considerable pyramidalization at boron [$\sum$(C-B-C) = 340(1)°] and a broad singlet in the

^{11}B NMR spectrum at 12 ppm ($\omega_{1/2} \approx 700$ Hz), characteristic of 4-coordinate boron. The B–Cl bond length in **1** is 0.1–0.3 Å shorter than those in Bourissou's metal-chloride-borane complexes (Table 1), consistent with the enhanced Lewis acidity of the $ArBPh_2$ acceptor in TXPB relative to an $ArBCy_2$ group (see Table 2 for key spectroscopic and crystallographic data for complexes **1–5**).

Table 1. Key crystallographic and spectroscopic values for structurally characterized literature complexes exhibiting a M–Cl–B bridging interaction (see Table 2 for [RhCl(CO)(TXPB)]).

Compound	M–Cl [Å]	B–Cl [Å]	M–Cl–B [deg]	∑(C-B-C) [deg]	^{11}B NMR [δ, ppm]	Reference
[{PdCl(TXPB)}$_2$]	2.362(2)	1.981(8)	104.0(2)	336	2	3
[(*p*-cymene)RuCl$_2${NC$_5$H$_4$(CH$_2$BCy$_2$)-*o*}][b]	2.419(2) 2.419(2)	2.156(11) 2.103(9)	111.0(3) 110.0(3)	346	22	5
[(η^3-allyl)PdCl{P^{i}Pr$_2$(C$_6$H$_4$)BCy$_2$-*o*}]	2.352(1)	2.165(2)	101.10(6)	349	47	6
[(NBD)RhCl{P^{i}Pr$_2$(C$_6$H$_4$)BCy$_2$-*o*}]	2.344(1)	2.117(2)	107.22(5)	343	26[a]	7
[PdCl$_2${P^{i}Pr$_2$(C$_6$H$_4$)BCy$_2$-*o*}]$_2$	2.263(2)	2.334(7)	NR	354	ND	7
[PdCl$_2$(PPh$_3$){P^{i}Pr$_2$(C$_6$H$_4$)BCy$_2$-*o*}]	2.280(1)	2.109(4)	111.94(12)	344	22	7
[{η^5-C$_5$H$_4$B(C$_6$F$_5$)$_2$}(Ind)TiCl$_2$]	2.4641(9)	2.007(4)	88.38(11)	342	4.8	8
[(κ^3-Tp)OsCl$_2$(NPhBPh$_2$)]	2.403(3)	2.069(15)	80.2(4)	347	NR	9
[(IMes)$_2$PtHCl{BC$_5$H$_3$(*o*-SiMe$_3$)(*p*-^{i}Pr)}]	N/A	N/A	N/A	N/A	36	10
[(IMes)$_2$PtHCl{BC$_5$H$_4$(SiMe$_3$)-*o*}]	N/A	N/A	N/A	N/A	39	10

a = solid-state NMR chemical shift; b = two different orientations of the molecule were present in the asymmetric unit cell; N/A = not applicable; ND = not detected.

Scheme 1. Preparation of complexes **1–3**.

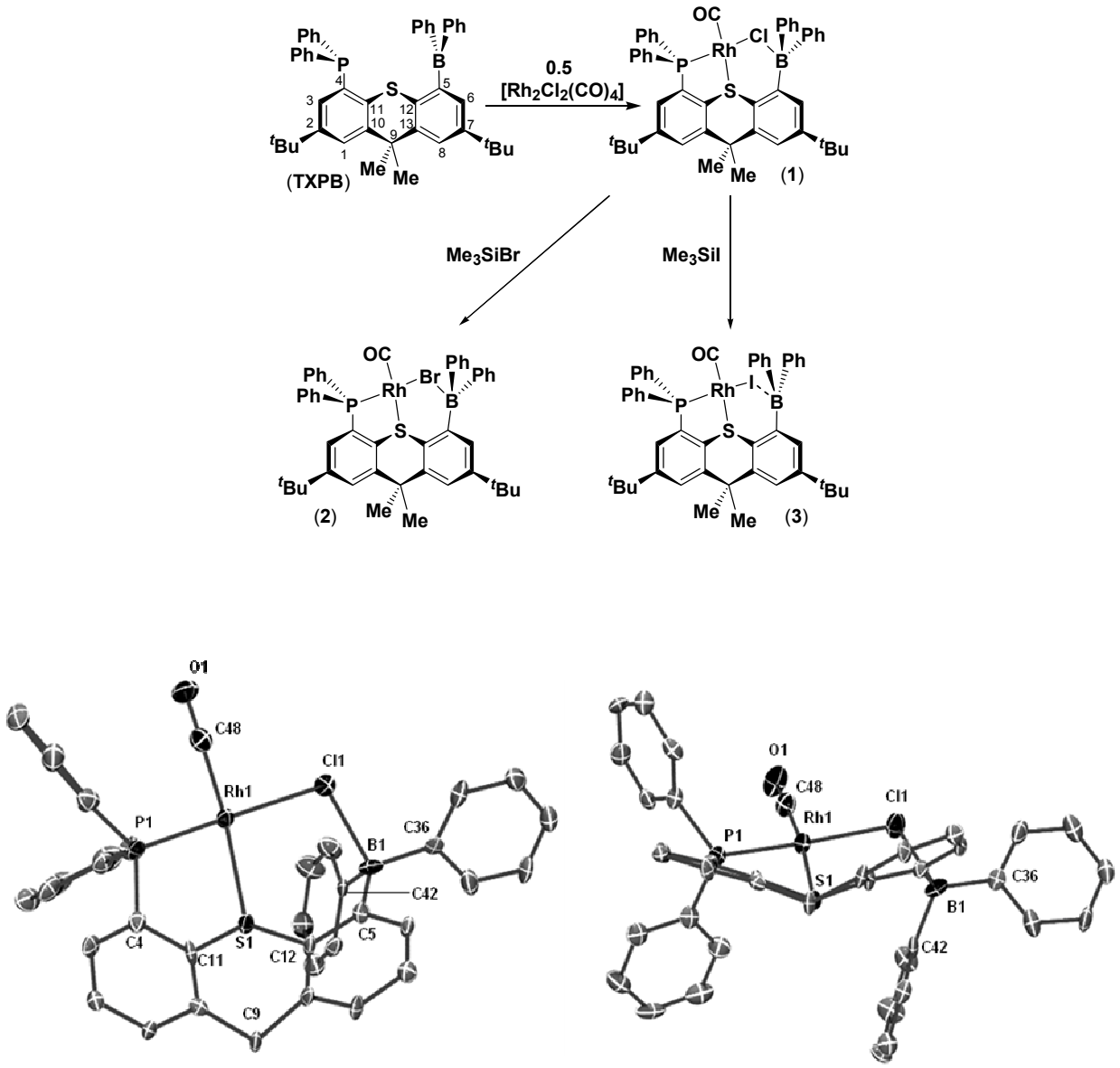

Figure 3. Solid-state structure of [RhCl(CO)(TXPB)]·hexane (**1**)·hexane with ellipsoids at 50% probability. *Tert*-butyl and C*Me*$_2$ methyl groups, hydrogen atoms, and solvent are omitted for clarity.

A Borane-Bearing Rhodium Bromo Carbonyl Complex. Substitution of the chloride co-ligand in **1** to form [RhBr(CO)(TXPB)] (**2**) was achieved using bromotrimethylsilane in CH_2Cl_2 (Scheme 1), providing complex **2** as an orange powder in 74% isolated yield. A doublet was observed in the ^{31}P NMR spectrum at 64.5 ppm ($^1J_{P,Rh}$ = 164.0 Hz), shifted 4.5 ppm to higher frequency of complex **1**. The CO stretching frequency is 2013 cm^{-1} in Nujol and 2008 cm^{-1} in CH_2Cl_2 by IR

spectroscopy; very similar values were reported for complex **1** [2010 cm^{-1}(Nujol); 2013 cm^{-1}(CH_2Cl_2)].[4] Complex **2**, like complex **1**, is fluxional in solution, giving a single resonance in the room temperature ^{1}H NMR spectrum for the CMe_2 group. At low temperature these methyl substituents become inequivalent with a coalescence temperature (T_c) of 211(2) K for **2** ($\Delta G^{\ddagger}$ at T_c = 39.7(5) kJ/mol).[26] For comparison, T_c for **1** is 254(2) K, leading to a value of 47.7(6) kJ/mol for $\Delta G^{\ddagger}$ at this temperature.

X-ray quality crystals of **2**·hexane were grown from a saturated solution of **2** in hexanes cooled to –30°C for several days (Figure 4, Tables 2-3). The X-ray crystal structure contains two independent molecules of **2** (A and B) within the unit cell. For both molecules, the geometry at rhodium is distorted square planar with S–Rh–CO and P–Rh–Br angles of 173.4(3)° and 176.34(6)° for molecule A, and 176.0(3)° and 169.56(5)° for molecule B; closely analogous S–Rh–CO and P–Rh–X angles were observed for complex **1**. In addition, both molecules of **2** exhibit a unique metal–bromide–borane interaction. However, molecules A and B differ in the position of the bromide anion with respect to the thioxanthene backbone; the C(12)–C(5)–B–Br torsion angle is 76.9(7)° in molecule A, and –43.3(9)° in molecule B [*cf.* 78.7(8)° in **1**]. Only one isomer was observed in the solution ^{1}H and ^{31}P NMR spectra of **2** down to –70 °C, and only one carbonyl stretch was observed in the IR spectrum of **2** in CH_2Cl_2 and Nujol. However, different orientations of the metal–halide bond relative to the TXPB ligand backbone must be involved in the fluxional process responsible for CMe_2 methyl group exchange.

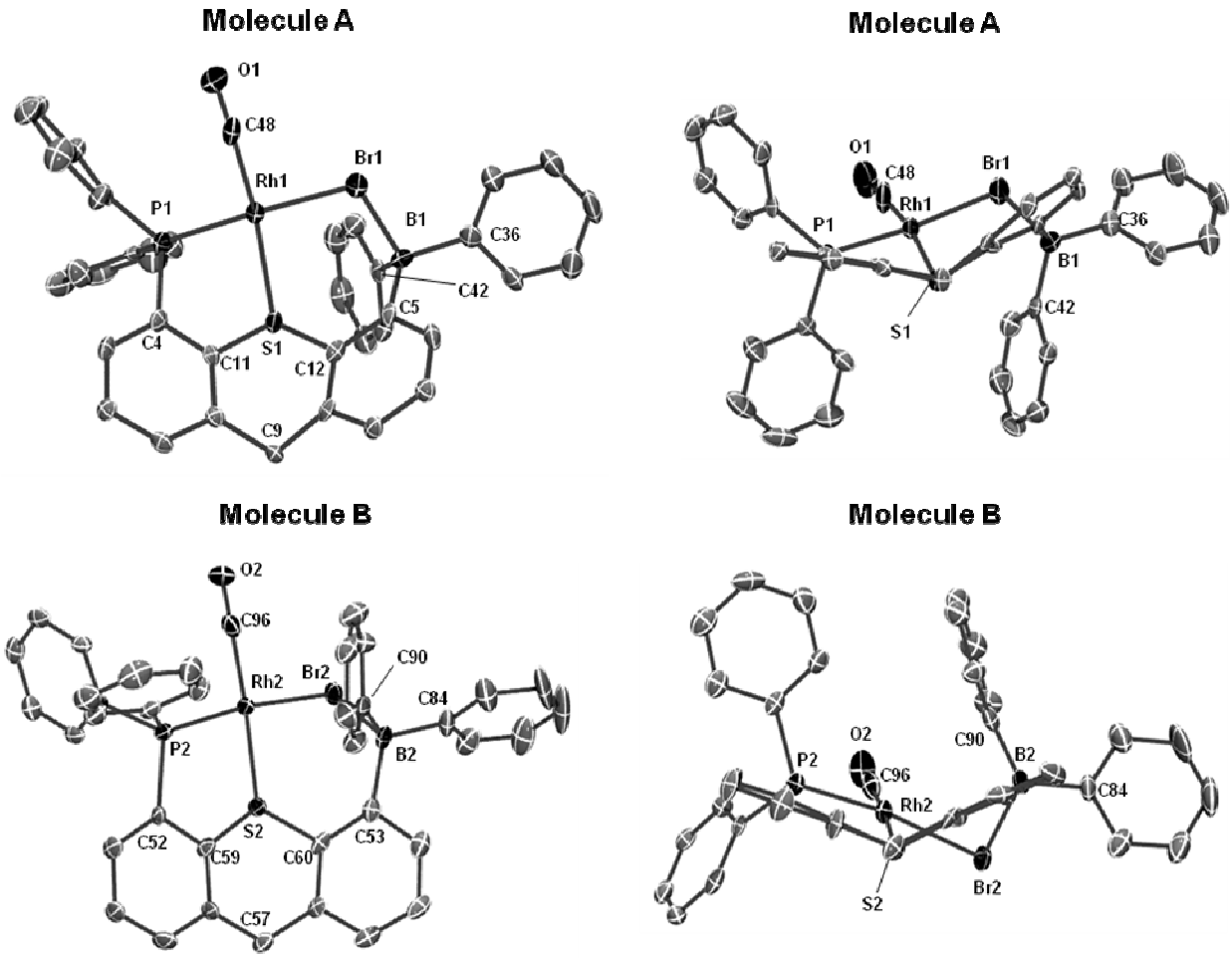

Figure 4. Solid-state structure of [RhBr(CO)(TXPB)]·hexane (**2**)·hexane with ellipsoids at 50% probability. *Tert*-butyl and C*Me*$_2$ methyl groups, hydrogen atoms, and solvent are omitted for clarity.

Due to the inequivalent metal–TXPB binding modes in molecules A and B, key bond lengths and angles in the two molecules are significantly different. For example, the B–Br distance in molecule A is 2.190(8) Å while that in molecule B is 2.267(9) Å. These distances are appreciably different from one another (see below for discussion), but are both approximately 0.2–0.3 Å longer than B–Br in the neutral Lewis acid–Lewis base adducts Ph_3PBBr_3 (1.978–2.013 Å),[27] $PyBBr_3$ (1.96–2.01 Å),[28] and $LBBr_2$, where L = 2-(dimethylaminomethyl)phenyl (2.01 and 2.02 Å),[29] highlighting the presence of a significant B–Br interaction in both A and B. The ^{11}B NMR signal for **2** (δ 27 ppm; $\omega_{1/2} \approx 900$ Hz) is also closer to that of **1** (12 ppm) than free TXPB (69 ppm),[2] substantiating the presence in solution of a significant B–Br interaction in **2**.

The Rh–Br and Rh–S distances in molecules A and B of **2** are also notably different; Rh–Br is 2.4519(11) Å in molecule A and 2.5161(11) Å in molecule B, while Rh–S is 2.380(2) Å in molecule A and 2.304(2) Å in molecule B. The shorter Rh–Br distance in *molecule A* is similar to those in closely related $[RhBr(CO)(PPh_3)_2]$ (2.453 Å)[30] and $[^nBu_4N][RhBr(NBD)(^iPr_2P(C_6H_4)BPh_3\text{-}p)]$ (NBD = norbornadiene) (2.465 Å).[31] However, Rh–Br in molecule B is more comparable with that in [RhBr(CO)(Me$_2$carbox)] [Me$_2$carbox = 1-(4,4-dimethyl-4,5-dihydrooxazol-2-yl)-3-mesitylimidazol-2-ylidene] (2.507 Å)[32] in which the bromo ligand experiences the high *trans*-influence of an *N*-heterocyclic carbene. By contrast, the Rh–S distance in *molecule B* is more similar to that in closely related borane-free complexes, while that in molecule A is significantly longer; Rh–S distances of 2.293 and 2.286 Å were reported for $[(nacnac^{Xyl})Rh(\kappa^1S\text{-dbt})_2]$ [$nacnac^{Xyl}$ = CH{C(Me)NXyl}$_2$; Xyl = $C_6H_3Me_2$-2,6; dbt = dibenzo[*b,d*]thiophene],[33] respectively, and Pd–S distances of 2.290 and 2.300 Å were reported for $[PdCl_2(L)]$ [L = 6-(4-hydroxy-2-phenylsulfanylphenoxy)-5,7-dioxa-6-phosphadibenzo[*a*,*c*]cycloheptene][34] and $[PdCl_2\{\kappa^2\text{-}PhS(C_6H_4)CH_2PPh_2\text{-}o\}]$,[35] respectively (*note:* the covalent radius of Pd is 1.39 Å *versus* 1.42 Å for Rh).[36]

A final key structural parameter in the description of complex **2** is the Rh–Br–B angle, which is 103.4(2)° in molecule A, but only 87.6(2)° in molecule B (*cf.* 104.6(3)° in **1**). Both the acute Rh–Br–B angle and the short Rh–S distance in molecule B are likely a consequence of the alternative binding mode of the rigid TXPB ligand. Elongation of both the Rh–Br and B–Br bonds in molecule B may perhaps be attributed to increased *p*-character in Rh–Br and B–Br coordination due to a Rh–Br–B angle constrained to less than 90°. For Al_2X_6 (X = Cl or Br), calculations have shown an ~0.01 Å increase in the bridging Al–X bond lengths upon narrowing of the Al–X–Al angle by only 4–5° (from close to 90° by bending of the $Al(X_{terminal})_2$ groups out of the plane with the two bridging halide ligands).[37]

Table 2. Spectroscopic and Crystallographic Data for Complexes **1–5**.

Complex	**1**	**2**	**3**	**4**	**5**[a]
Metal and co-ligands	Rh Cl CO	Rh Br CO	Rh I CO	Rh F CO	Rh CO

		Molecule A	Molecule B[i]			Cation
^{31}P NMR [δ, ppm]	60.0	64.5		67.2	52.2	64.9
^{11}B NMR [δ, ppm]	12	27		56	4	57
^{19}F NMR [δ, ppm]	---	---		---	-186	---
$^{1}J_{P,Rh}$ [Hz]	161.3	164.0		166.8	166.2	166.8
$^{1}J_{C,Rh}$ / $^{2}J_{C,P}$ for *C*O [Hz]	77/18	77/15		74/14	75/19	72/13
$^{2}J_{P,F}$ [Hz]	---	---		---	6.2	---
ν(CO)(CH_2Cl_2/Nujol) [cm^{-1}]	2013/2010	2008/2013		2002/2004	2011/2008	2038/2028
T_c for C*Me*$_2$ exchange (K)[b]	254(2)	211(2)		210(2)	274(2)	312(2)
$\Delta G^{\ddagger}$ at T_c ($kJmol^{-1}$)[b]	47.7(6)	39.7(5)		39.5(5)	51.5(7)	61.2(8)
Rh–X [Å]	2.381(2)	2.4519(11)	2.5161(11)	2.6640(7)	3.261(3)	---
Rh–C_{ortho} [Å]	---	---	---	---	2.564(5)	2.797(3)
Rh–C_{ipso} [Å]	---	---	---	---	2.336(4)	2.362(2)
Rh···B [Å]	3.470	3.647(9)	3.316(9)	3.502(7)	3.231(5)	2.557(3)
Rh–CO [Å]	1.817(11)	1.829(8)	1.841(7)	1.855(7)	1.816(5)	1.870(3)
Rh–P [Å]	2.205(2)	2.202(2)	2.196(2)	2.2237(14)	2.2176(13)	2.2394(7)
Rh–S [Å]	2.379(2)	2.3797(17)	2.3044(17)	2.2997(14)	2.4045(12)	2.3234(6)
B–X [Å]	1.995(9)	2.190(8)	2.267(9)	3.125(7)	1.445(6)	---
Rh–X–B [deg]	104.6(3)	103.4(2)	87.6(2)	73.96(12)	76.0(2)	---
S–Rh–CO [deg]	171.3(3)	173.4(3)	176.0(3)	163.8(2)	168.02(17)	172.48(9)
P–Rh–X [deg]	172.64(8)	176.34(6)	169.56(5)	169.58(4)	---	--
P–Rh–$CC_{(cent)}$/$BC_{(cent)}$ [c]	---	---	---	---	160.53(16)	154.20(9)
Rh–(PCCSplane) [Å][d]	1.023	0.988	0.271	0.144	1.226	0.531
∑(C-B-C) [deg]	340(1)	342(1)	339(1)	356.8(9)	331.2(7)	358.6(4)
B–(CCCplane) [Å][e]	0.426	0.397	0.437	0.164	0.518	0.110
S–C(12)–C(5)–B [deg][f,g]	–13.3(10)	–14.8(9)	13.0(11)	16.6(8)	1.1(6)	4.9(3)
C(12)–C(5)–B–X [deg][f,g]	78.7(8)	76.9(7)	–43.3(9)	–53.1(6)	–46.5(6)	---
Ligand Bend [deg][g]	42.8	42.4	47.9	52.9	41.6	54.1

(a) NMR spectroscopic data for complex **5** is for the cation only. (b) T_c is the coalescence temperature and $\Delta G^{\ddagger}$ is for C*Me*$_2$ methyl exchange. (c) $CC_{(cent)}$ and $BC_{(cent)}$ represent the centroid position between C(42)–C(43) and B(1)–C(42), respectively. (d) PCCSplane = P(1)–C(4)–C(11)–S(1). (e) CCCplane = C(5)–C(36)–C(42). (f) Torsion angles are for the molecules as shown in Figures 3–5, 6 and 8. (g) Positive torsion angles indicate that boron or the B–X bond is oriented up into the fold of the thioxanthene backbone. (h) Ligand Bend = the angle between the C(1)–C(2)–C(3)–C(4)–C(10)–C(11) and C(5)–C(6)–C(7)–C(8)–C(12)–C(13) planes (an angle of 0° would correspond to a planar

thioxanthene backbone). (i) Molecule B of complex **2** uses a different numbering scheme; substitute B(1), P(1), C(1)-C(13),C(36), C(42) and C(43) for B(2), P(2), C(49)-C(61), C(84), C(90) and C(91).

A Borane-Bearing Rhodium Iodo Carbonyl Complex. Treatment of complex **1** with iodotrimethylsilane provided [RhI(CO)(TXPB)] (**3**) (Scheme 1) as a rust-red powder in 83% isolated yield. The ^{31}P NMR spectrum of **3** consists of a doublet at 67.2 ppm ($^{1}J_{P,Rh}$ = 166.8 Hz), shifted 7.2 ppm to higher frequency of complex **1**. A very broad singlet at 56 ppm ($\omega_{1/2} \approx$ 1800 Hz) was observed in the ^{11}B NMR spectrum, which is shielded by only 13 ppm relative to free TXPB, consistent with a weak B···I interaction. As with **2**, complex **3** is fluxional in solution, evidenced by chemically equivalent C*Me*$_2$ methyl-substituents in the ^{1}H NMR spectrum at room temperature (coalescence temperature = 210(2) K). The $\Delta G^{\ddagger}$ value for C*Me*$_2$ methyl group exchange at T_c is 39.5(5) kJ/mol, which is equal within error to $\Delta G^{\ddagger}$ for complex **2** (39.7(5) kJ/mol at 211(2) K).

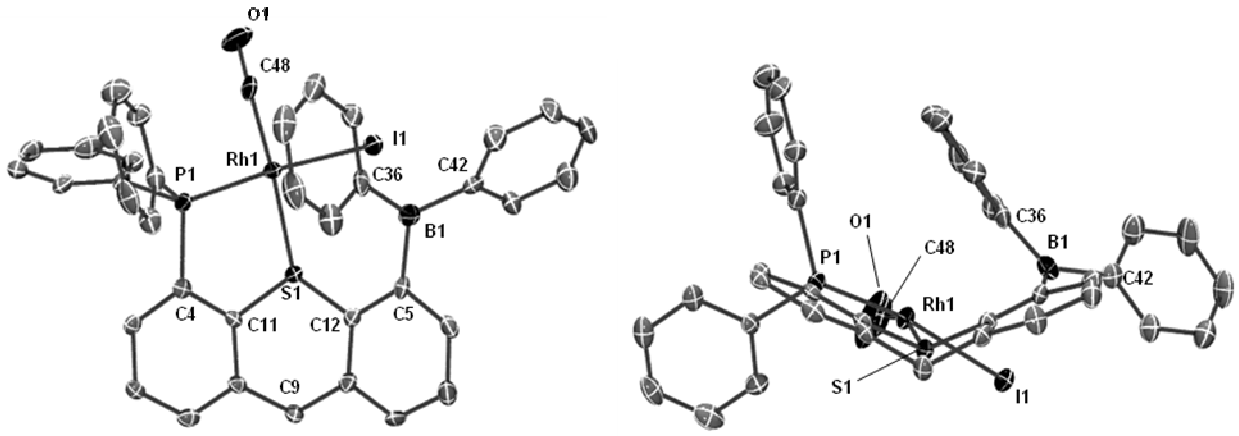

Figure 5. Solid-state structure of [RhI(CO)(TXPB)]·hexane (**3**)·hexane with ellipsoids at the 50% probability level. *Tert*-butyl and C*Me*$_2$ methyl groups, hydrogen atoms, and solvent are omitted for clarity.

X-ray quality crystals of **3**·hexane were obtained by cooling a saturated solution of **3** in hexanes to –30°C for several days (Figure 5, Tables 2-3). The S–Rh–CO and P–Rh–I bond angles are 163.8(2)°

and 169.58(4)°, respectively, highlighting a substantially distorted square planar geometry. The Rh–P and Rh–CO bond distances are 2.2237(14) and 1.855(7) Å, respectively; Rh–P is slightly longer in **3** than in **1** and **2** (Table 2), consistent with the higher *trans*-influence of iodide relative to chloride and bromide,[38] and the absence of a strong halide–borane interaction in **3**. The orientation of iodide relative to the thioxanthene backbone of **3** is analogous to that in molecule B in the unit cell of **2**, with a C(12)–C(5)–B–I torsion angle of –53.1(6)°. As a consequence, the Rh–S distance is 2.2997(14) Å, which is similar to that in molecule B of complex **2**, but much shorter than those in complex **1** and molecule A of complex **2** (Table 2). The Rh–I–B bond angle in **3** is also extremely acute [73.96(12)°]. A similar situation was observed in molecule B of **2** [Rh–I–B = 87.6(2)°], while the Rh–X–B angles are 103–105° in complex **1** and molecule A of **2**. The more acute Rh–X–B angle in **3**, relative to that in molecule B of complex **2**, is likely the result of a longer Rh–X bond and the absence of a strong halide-borane interaction in **3**.

The Rh–I bond distance of 2.6640(7) Å compares well to those in similar rhodium compounds, where an iodide is bound *trans* to a phosphine. These compounds include [{(S)-diop} $Rh(PPh_3)I$] [(S)-diop = (S)-2-(diphenylphosphino)-2'-methoxy-1,1'-binaphthyl][39] and [(BINAP)Rh(CO)I] [BINAP = 2,2'-bis(diphenylphosphino)-1,1'-binaphthyl],[40] with Rh–I bond distances of 2.704 and 2.686 Å, respectively. However, a key feature of complex **3** is the extremely long B···I distance of 3.125(7) Å, which is approximately 0.8–0.9 Å longer than B–I distances in the Lewis acid–Lewis base adducts $Me_2NCHO–BI_3$ (2.224–2.262 Å),[41] (IEtC=CEt)BI_2–Py (2.275, 2.294 Å)[42] and $Me_3P–BI_3$ (2.237–2.272 Å).[43] The long B···I distance in **3** may be attributed to the incompatibility of a hard borane Lewis acid with a soft iodide anion (B–X bond strengths decrease in the order F > Cl > Br > I, and no iodoborate anions have been structurally characterized to-date), in combination with an extremely acute Rh–I–B angle. In keeping with the long B···I distance and the high frequency ^{11}B NMR chemical shift, boron in **3** is very nearly planar [$\sum$(C-B-C) = 356.8(9)°].

The CO stretching frequency for **3** (2004 cm^{-1} in Nujol and 2002 cm^{-1} in CH_2Cl_2) is significantly lower than those in complexes **1** and **2**, indicating increased electron density at the metal. In related

series of d^8 complexes with *cis*-disposed halide and carbonyl ligands, the CO stretching frequency is effectively unchanged after substitution of chloride for iodide; see for example [(BINAP)Rh(CO)X] (X = Cl or I)[40] and [Rh(DTBPMB)X(CO)] [X = Cl or I; DTBPMB = 1,2-(^{t}Bu$_2$PCH$_2$)$_2$C$_6$H$_4$].[44] The lower CO stretching frequency for **3** relative to **1** and **2** is therefore consistent with less effective donation from the halide to the metal centre in **1** and **2** as a result of halide–borane coordination. However, all or part of the shift in ν(CO) could also be due to predominance of a different TXPB bonding mode in complex **3** with a shorter Rh–S distance (as observed in the solid state structure). It is therefore not possible to draw any definite conclusions from this data.

Table 3. Crystallographic Data Collection and Refinement Parameters for Complexes **1–5**.

Structure	**1** · hexane	**2** · hexane	**3** · hexane	**4** · 1.5CH_2Cl_2	**5** · CH_2Cl_2
formula	$C_{54}H_{62}BClOPRhS$	$C_{54}H_{62}BBrOPRhS$	$C_{54}H_{62}BIOPRhS$	$C_{49.5}H_{51}BCl_3FOPRhS$	$C_{49}H_{50}BCl_2F_6OP_2RhS$
formula wt	939.24	983.70	1030.69	964.00	1047.51
T (K)	173(2)	100(2)	100(2)	100(2)	173(2)
cryst. syst.	Monoclinic	Triclinic	Monoclinic	Triclinic	Triclinic
space group	*P*2(1)/*n*	*P*-1	*P*2(1)/*c*	*P*-1	*P*-1
a (Å)	13.773(3)	13.784(4)	20.985(5)	10.480(2)	13.7285(11)
b (Å)	20.799(5)	16.784(4)	10.931(2)	14.606(3)	13.7787(10)
c (Å)	17.532(5)	22.340(6)	21.318(4)	15.417(3)	14.0510(11)
α [deg]	90	78.308(5)	90	84.035(4)	69.0590(10)
β [deg]	103.832(5)	72.860(5)	94.691(4)	81.671(4)	84.6330(10)
γ [deg]	90	87.227(5)	90	76.197(4)	83.8570(10)
volume [Å^3]	4877(2)	4836(2)	4873.7(18)	2261.7(8)	2463.7(3)
Z	4	4	4	2	2
density (calcd; mg/m^3)	1.279	1.351	1.405	1.416	1.412
μ (mm^{-1})	0.517	1.293	1.097	0.677	0.620
F(000)	1968	2040	2112	994	1072
crystal size (mm^3)	0.35×0.04×0.03	0.28×0.13×0.05	0.17×0.10× 0.04	0.22×0.16×0.03	0.58×0.22×0.08
θ range for collection [deg]	1.70–18.15	1.55–26.57	1.92–25.64	1.34–26.5	1.55–30.51
no. of reflns collected	13733	42443	37759	26414	36404
no. of indep Reflns	3396	19853	9041	9232	14662
completeness to θ max (%)	98.9	98.2	98.2	98.4	97.5

absorption correction	Analytical	Numerical	Numerical	Numerical	Numerical
max and min transmission	0.9846, 0.8396	0.9382, 0.7135	0.9575, 0.8355	0.9800, 0.8653	1.000, 0.712
GOF on F^2	1.116	0.885	0.936	0.970	1.049
Final R_1 [$I > 2\sigma(I)$] (%)	3.79	7.22	4.86	5.69	4.53

Zwitterionic [Rh(CO)(TXPB–F)]. Treatment of **1** with $[NMe_4]F$ in CH_2Cl_2 gave [Rh(CO)(TXPB–F)] (**4**) [TXPB–F = {5-(2,7-di-*tert*-butyl-4-diphenylphosphino-9,9-dimethylthioxanthenyl)}diphenylfluoroborate] as an orange-red powder in an isolated yield of 72% (Scheme 2). Reaction of **1** with $[NBu_4][Ph_3SiF_2]$ provided an alternative route to complex **4**, but due to the formation of similarly soluble Ph_3SiF as a reaction byproduct, isolation of pure **4** via this method proved problematic. Complex **4**, unlike **1–3** is not thermally stable at room temperature, being substantially decomposed after 24 hours in solution (CH_2Cl_2). A key spectroscopic feature for complex **4** is a singlet in the ^{11}B NMR spectrum at 4 ppm ($\omega_{1/2} \approx 350$ Hz), characteristic of 4-coordinate boron, and shifted 8 ppm to lower frequency of **1**, indicating the presence of a very strong B–F interaction. Moreover, a broad singlet was observed in the ^{19}F NMR spectrum at –186 ppm ($\omega_{1/2} \approx 180$ Hz), characteristic of fluorine bound to quadrupolar boron. These NMR data compare well with the related triarylfluoroborate compounds $[FB(C_6F_5)_2\{C_6F_4(P^iPr_3)\text{-}p\}]$ (^{11}B NMR δ –0.89 ppm; ^{19}F NMR δ –191.37 ppm),[45] $[F(Tip)B(C_6H_4\text{-}o)_2PMe_2]$ (Tip = 2,4,6-triisopropylphenyl) (^{11}B NMR δ 3.7 ppm; ^{19}F NMR δ –162.44 ppm),[46] and [K{[2.2.2]-cryptand}][FB(Ant)$_3$] (Ant = 9–anthracenyl) (^{11}B NMR δ 6.04 ppm; ^{19}F NMR δ –133.32 ppm).[47]

Scheme 2. Preparation of Complexes **4** and **5**.

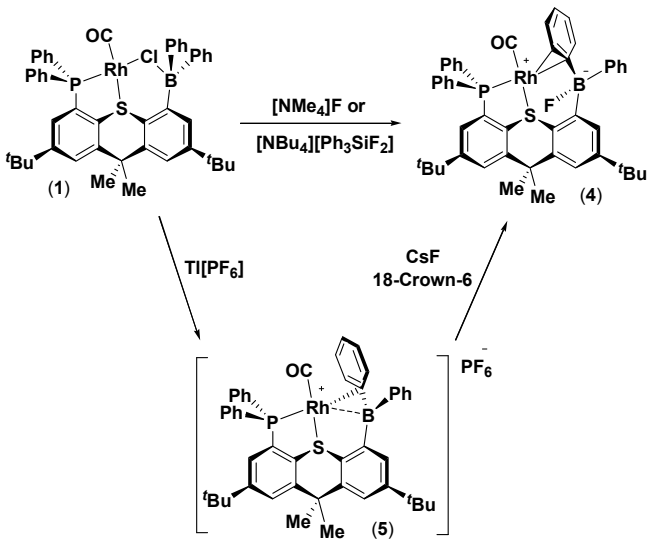

X-ray quality crystals of **4**·1.5CH_2Cl_2 were grown by slow diffusion of hexanes into a solution of **4** in CH_2Cl_2 at –30°C. In the solid-state, as was observed spectroscopically in solution, the fluoride ligand does not form a strong interaction with the metal centre (Figure 6, Tables 2-3). Rather, it binds preferentially to boron producing a zwitterionic complex containing a 4-coordinate anionic borate and a cationic rhodium centre. The B–F bond distance in **4** is 1.445(6) Å, which lies at the shorter end of the range for B–F bond distances in fluoroborates such as $[CPh_3][FB\{C_6F_4(C_6F_5)\text{-}o\}_3]$ (1.472 Å),[48] $[FB(Mes)_2Ar]$ [Ar = 1-(8-(trimethylammonio)methylnaphthalene)] (1.486 Å),[49] and $K[FB(Ph)(CF_3)_2]$ (1.452 Å).[50] Boron in **4** also exhibits a greater degree of pyramidalization [$\sum$(C-B-C) = 331.2(7)°] than that in compounds **1**-**3** (Table 2). The Rh···F distance of 3.261(3) Å in complex **4** is well outside of the sum of the atomic radii for the two elements (1.99 Å),[36] and approaches the sum of the Van der Waals radii (3.51 Å).[51]

To complete a highly distorted square planar geometry at rhodium [S–Rh–CO = 168.02(17)°, P–Rh–*cent* = 160.53(16)°; *cent* = the centroid position between C_{ipso} and C_{ortho}], a phenyl ring in the $FBAr_3$ unit is η^2-bound to rhodium via the *ipso*- and *ortho*-carbon atoms. The Rh–C_{ipso} distance of 2.336(4) Å in **4** is comparable with those in other rhodium(I) complexes featuring an η^2-bound aryl ring, including $[Rh(CO)(POPheph)][ClO_4]$ [POPheph = κ^1-$PPh_2POCH(Ph)CH(Me)NMe\{CH(Ph)(\eta^2\text{-}Ph)\}$] (2.334 Å)[52] and $[Rh(PEt_3)_2\{\kappa^1\text{-}OC(Ph_2)(\eta^2\text{-}Ph)\}]$ (2.350 Å).[53] By contrast, the Rh–C_{ortho} distance of 2.564(5) Å in **4**

is significantly longer (*cf.* 2.449 Å and 2.398 Å, respectively, in the literature complexes above), indicative of a weaker interaction.

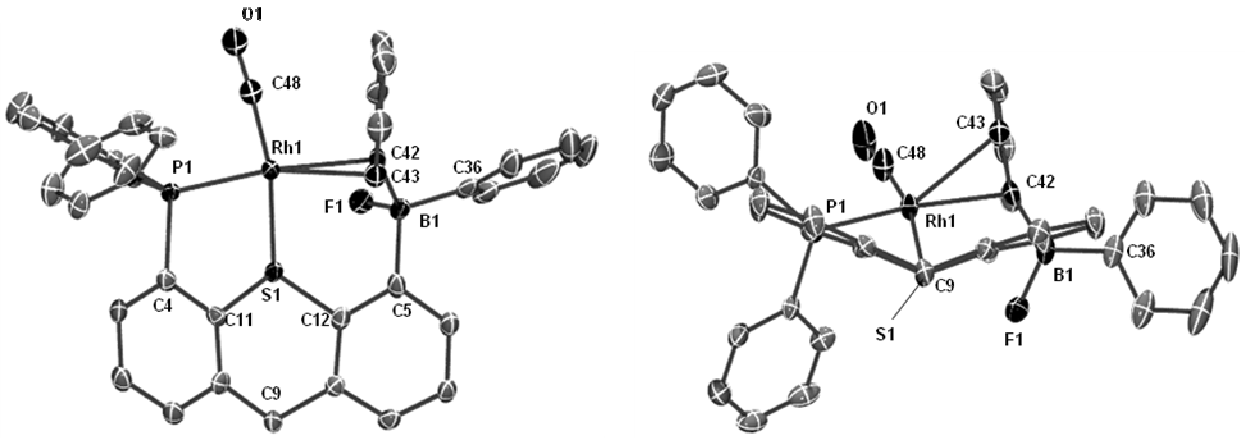

Figure 6. Solid-state structure of [Rh(CO)(TXPB–F)]·1.5CH_2Cl_2 (**4**)·1.5CH_2Cl_2 with ellipsoids at 50% probability. *Tert*-butyl and C*Me*$_2$ methyl groups, hydrogen atoms, and solvent are omitted for clarity.

Fluxional NMR Behavior of [Rh(CO)(TXPB–F)]. Despite η^2-arene coordination in the solid state, complex **4** is fluxional in solution at room temperature; the C*Me*$_2$ methyl groups of the thioxanthene backbone are equivalent [although a coalescence temperature of 274(2) K ($\Delta G^{\ddagger}$ at T_c = 51.5(7) kJ/mol) for C*Me*$_2$ methyl group exchange does suggest a higher activation barrier for this process in **4**, compared with complexes **1–3** (assuming that $\Delta S^{\ddagger}$ is not large and negative)], and the phenyl rings on both boron and phosphorus undergo pairwise exchange. At –50 °C, two distinct *B*-phenyl and *P*-phenyl rings are observed, but the *ortho* and *meta* C*H* positions of each ring remain equivalent down to –80 °C. Given the complexity of the aryl region in complex **4**, this assignment was verified by low-temperature 2D COSY and DEPT–135 NMR spectroscopy of ***d*$_{10}$-4** in which both *P*-phenyl rings are perdeuterated (Figure 7). The exchange process responsible for equivalence of the *ortho* and *meta* positions on each of the two *B*-phenyl rings (while maintaining inequivalence of the C*Me*$_2$ methyl, *B*-phenyl and *P*-phenyl groups) in **4** must involve rotation around the B–C bonds. This would require loss of any η^2-arene interaction, presumably with pivoting about B(1)–C(5) (see Figure 8)

to position the previously coordinated *B*-phenyl ring further from rhodium and bring fluorine into closer proximity with the metal. The η^2-arene interactions in [Rh(CO)(POPheph)][ClO_4] and [Rh(PEt_3)$_2${κ^1-$OCPh_2$(η^2-Ph)}] (*vide supra*) also are not maintained on the NMR timescale in solution at room temperature.[52,53]

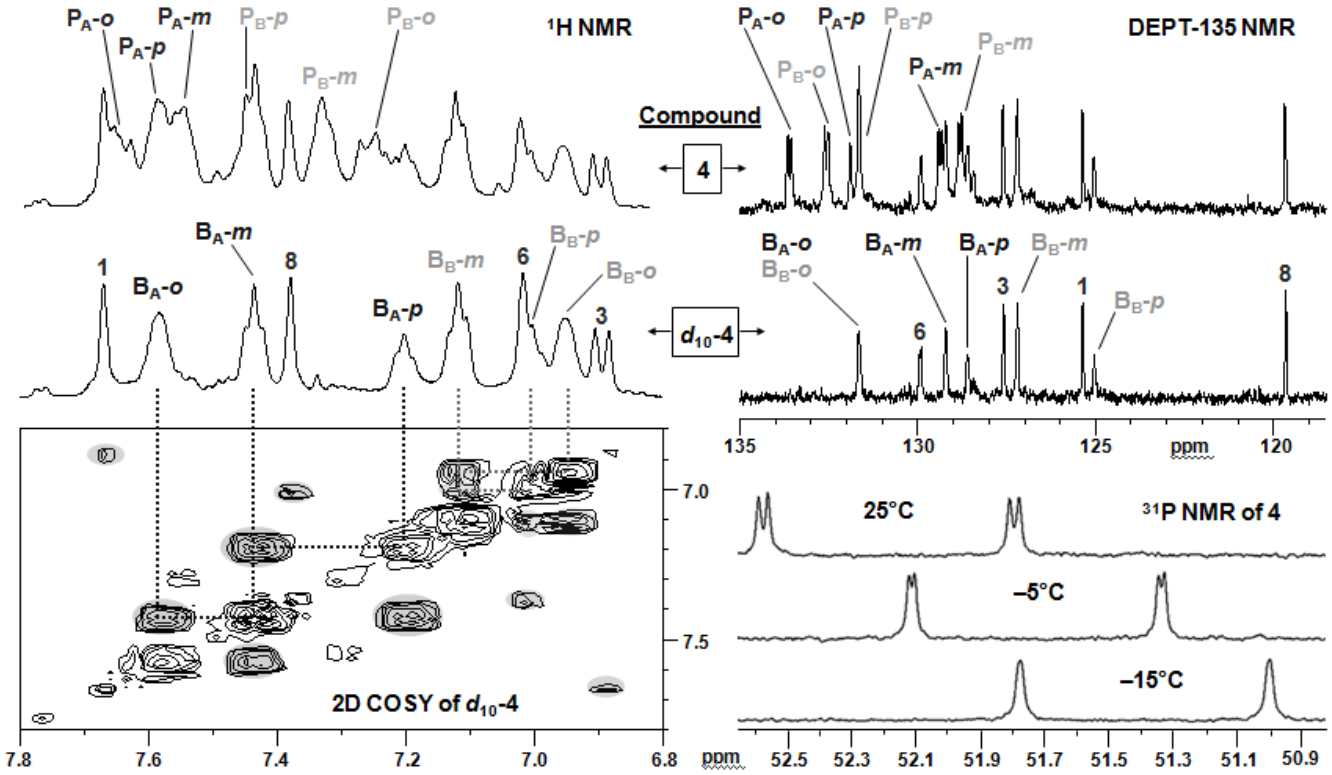

Figure 7. Aromatic regions of the ^{1}H and DEPT-135 NMR spectra of **4** and ***d*$_{10}$-4** at –50 °C. Aromatic region of the 2D COSY NMR spectrum for ***d*$_{10}$-4** at –50 °C, and ^{31}P NMR spectra for **4** at 25, –5, and –15 °C. All NMR spectra are in CD_2Cl_2.

^{31}P–^{19}F NMR Coupling and ν(CO) in [Rh(CO)(TXPB–F)]. Interestingly, despite the long P···F distance of 4.830(3) Å in the X-ray crystal structure of **4**, ^{31}P–^{19}F coupling is observed in the solution ^{31}P NMR spectrum at room temperature (δ 52.2 ppm; $^1J_{P,Rh}$ = 166 Hz, $J_{P,F}$ = 6.2 Hz; Figure 7). This small coupling could potentially occur via a through-bond or a through-space mechanism. For comparison, the *trans*-$^2J_{P,F}$ coupling constants in borane-free rhodium(I) fluoride complexes such as

[$RhF(PPh_3)_3$], [$RhF(PPh_3)_2(PPh_2F)$], and [$Rh_2(\mu\text{-}F)_2(PPh_3)_4$] are 172, 217 and 196 Hz, respectively, and the *cis*-$^2J_{P,F}$ coupling constants for [$RhF(PPh_3)_3$] and [$RhF(PPh_3)_2(PPh_2F)$] are 28.5 and 27 Hz, respectively.[54]

Through-space coupling in solution (direct spin-spin coupling) is a result of non-bonding interactions between lone pairs, and decreases in strength rapidly as the distance between coupling nuclei exceeds the sum of the van der Waals radii.[55] For example, in various tetrakis(diphenylphosphino)ferrocene ligands, ^{31}P–^{31}P through-space coupling was observed only at P···P distances of 4.9 Å and below.[56,57] In addition, for a range of rigid fluorine-containing compounds, ^{19}F–^{19}F through-space coupling was found to decay exponentially with increasing F···F distance, falling to 2 Hz at an F···F distance of 4.2 Å.[58] Similarly, in triflone-bearing phosphoramidite ligands, through-space ^{19}F–^{31}P coupling was calculated (using $Me_2NP(OH)_2\cdots F_4C$ as a model) to be significant only at distances below 4.0–4.9 Å,[59] depending on the angle between the interacting phosphorus lone pair and the trifluoromethyl group.[60]

These couplings represent an ideal situation involving lone pair–lone pair interactions, but in compound **4**, the lone pair on phosphorus is bound to rhodium. Hierso *et al.* have reported that in [($\kappa^2P^1P^2$-L)MX_2] (M = Ni and Pd; L = 1,1',2,2'-tetrakis(diphenylphosphino)-4,4'-di-*tert*-butylferrocene; X = Cl or Br), through-space coupling can be transmitted via an interaction between a free phosphine lone pair and the metal-phosphine bonding pair. However, the *trans*-annular through-space J_{PP} couplings in [($\kappa^2P^1P^2$-L)$PdCl_2$] are only 24.0 and 6.4 Hz, despite relatively short P···P distances of 3.8 and 4.4 Å, respectively. Based on these and other *trans*-annular J_{PP} coupling constants, Hierso *et al.* concluded that lone pair–bonding pair interactions are less effective for transmission of through-space coupling than lone pair–lone pair interactions (due to reduced directionality in the former).[57]

Based on the long P···F distance in the X-ray crystal structure of **4**, the strong angular dependence of through-space coupling,[59,61] and the requirement for coupling to occur via a lone pair–bonding pair interaction rather than a lone pair–lone pair interaction, through-space coupling in **4** seems unlikely. However, it is interesting to note that the magnitude of the $J_{P,F}$ coupling decreases with decreasing

temperature ($J_{P,F}$ = 6.2, 5.1, 4.3, 3.5, 2.7, 1.4 and 0 Hz at 25, 15, 10, 5, 0, –5, and –15 °C, respectively; Figure 7). Significant temperature dependencies (positive and negative) have been observed for through-space couplings in molecules of intermediate rigidity, where the observed coupling is a time-averaged value from all accessible solution conformations. For example, positive temperature dependencies were reported for through-space coupling in a triflone-bearing phosphoramidite ($J_{P,F}$ = 6.5 Hz at 100 °C and 1.7 Hz at –58 °C),[60] $P(C_6H_4CF_3\text{-}o)_xPh_{(3-x)}$ (x = 1-3; for x = 2, $J_{P,F}$ = 54.5 Hz at 117 °C and 51.1 Hz at –43 °C), [62] $C_6H_4F(CF_3)$-*o* ($J_{F,F}$ = 13.7 Hz at 97 °C and 11.2 Hz at –62 °C)[63] and $C_6H_4(CF_3)(SeCN)$-*o* ($J_{F,Se} \approx$ 51 Hz at 80 °C and 42 Hz at –40 °C),[64] while a large negative temperature dependency was reported for through-space coupling in $C_6H_4(CH_2F)(SeCN)$-*o* ($J_{F,Se} \approx$ 77 Hz at 20 °C and 104 Hz at –90 °C).[64,65] The $J_{P,F}$ coupling in **4** could therefore be assigned as a through-space coupling facilitated by solution conformations with P···F distances significantly shorter than that in the X-ray crystal structure of **4**. However, an alternative and perhaps more likely explanation is tighter (entropically favored) η^2-arene binding to rhodium at lower temperatures, leading to an increase in the average Rh···F distance (due to rotation about the C(5)–B bond) and a reduction in the magnitude of through-bond $^2J_{F,P}$ coupling.

A final important spectroscopic parameter for **4** is the CO stretching frequency, which is 2008 cm^{-1} in Nujol and 2011 cm^{-1} in CH_2Cl_2. Zwitterionic **4** might be expected to exhibit a significantly higher carbonyl stretching frequency than neutral **1** and **2**, but instead the frequencies are comparable (Table 2). The following factors must therefore compensate for the increase in positive charge at rhodium: (1) the η^2-interaction between rhodium and a phenyl ring of the fluoroborate group in TXPB–F, and (2) enhanced electron donor properties of an anionic TXPB–F ligand relative to neutral TXPB. Substantially more effective electron-donation has previously been reported for anionic $R_2B(CH_2PR'_2)_2^-$ and *m*-$Ph_3B(C_6H_4)P^iPr_2^-$ ligands relative to neutral $R_2Si(CH_2PR'_2)_2$ and *m*-$Ph_3Si(C_6H_4)P^iPr_2$ analogues.[31,66]

Cationic [Rh(CO)(TXPB)][PF$_6$]. A halide-free rhodium-TXPB cation was targeted to gain additional insight into the electronic environment in zwitterionic **4**. Treatment of **1** with Tl[PF_6] in CH_2Cl_2 yielded [Rh(CO)(TXPB)][PF_6] (**5**) as bright orange crystals in an isolated yield of 92%.

Complex **5** is the fluoride-free and formally cationic cousin of zwitterionic **4**, so sonication of **5** with CsF and 18-Crown-6 in CH_2Cl_2 provides an alternative route to **4** (Scheme 2). The ^{31}P NMR spectrum of **5** shows a doublet at 64.9 ppm ($^1J_{P,Rh}$ = 166.8 Hz), which is shifted 12.7 ppm to higher frequency of complex **4** (Table 2). In solution, exchange of the C*Me*$_2$ groups in **5** is slow, as was observed for complex **4**; the coalescence temperature for C*Me*$_2$ exchange in **5** is 312(2) K, leading to a $\Delta G^{\ddagger}$ of 61.2(8) kJ/mol at this temperature.

X-ray quality crystals of **5** (Figure 8, Tables 2-3) were grown from CH_2Cl_2/hexane at –30°C, and reveal a T-shaped arrangement of the phosphine, thioether and carbonyl groups [OC–Rh–S = 172.48(9)°, OC–Rh–P = 88.35(9)°, P–Rh–S = 84.84(2)°]. In addition, close approach of boron and the *ipso*-carbon of one *B*-phenyl ring to rhodium is observed [Rh–B = 2.557(3) Å and Rh–C(42) = 2.362(2) Å]. A weak interaction between rhodium and the *ortho*-carbon of the coordinated *B*-phenyl ring is also plausible based on the Rh–C(43) distance of 2.797(3) Å. However, pairwise equivalence of the *ortho* and *meta* positions of each *B*-phenyl ring in the solution ^1H and ^{13}C NMR spectra, even at –80 °C, argues against a significant Rh–C$_{ortho}$ interaction. For comparison, two *CH*$_{ortho}$ and two *CH*$_{meta}$ environments were observed for the coordinated *B*-phenyl ring in the low temperature ^1H and ^{13}C NMR spectra of the η^3-arylborane complexes [Pd(TXPB)], [Ni(TXPB)][3] and [Cp(CO)Fe(μ-CO)$_2$Rh(TXPB)].[4] The metal–arylborane interaction in **5** is therefore best considered to involve η^2*BC*-coordination. This assignment is supported by the observation of a broad singlet at 57 ppm ($\omega_{1/2} \approx$ 1800 Hz) in the ^{11}B NMR spectrum of **5**, which is shifted 12 ppm to low frequency of free TXPB, consistent with the presence of a significant, albeit weak, Rh–B interaction (*vide infra*).

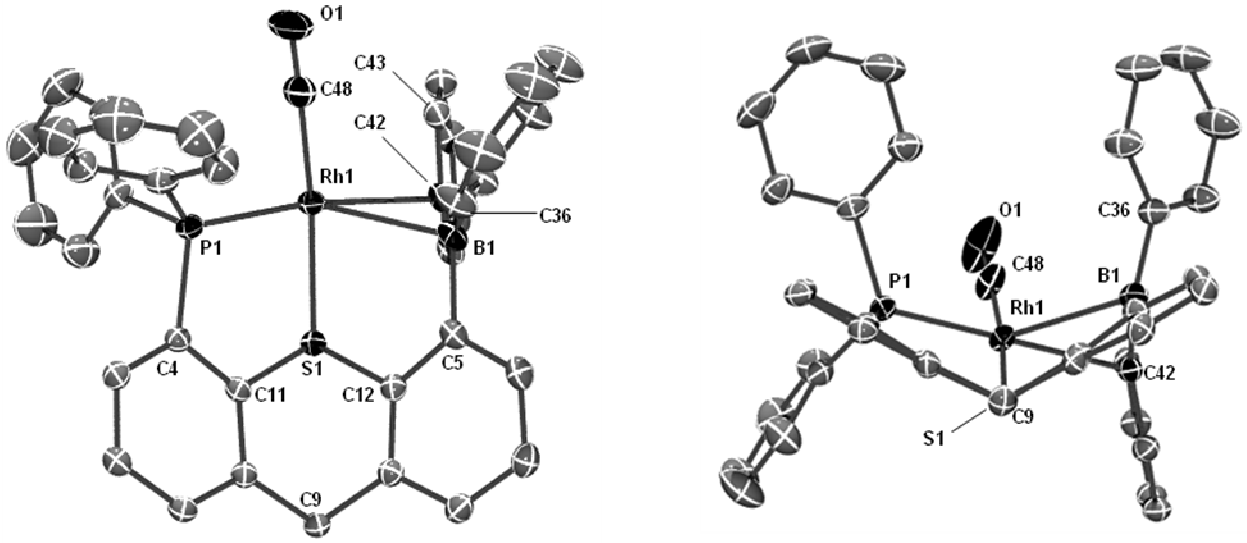

Figure 8. Solid-state structure of $[Rh(CO)(TXPB)][PF_6]\cdot CH_2Cl_2$ (**5**)$\cdot CH_2Cl_2$ with ellipsoids at the 50% probability level. *Tert*-butyl and C*Me*$_2$ methyl groups, the PF_6 counteranion, hydrogen atoms, and solvent are omitted for clarity.

Both η^1*B*- and η^3*BCC* coordination modes have previously been reported in metal arylborane complexes (*vide supra*), and the relationship between these arylborane coordination modes parallels that between η^1-benzyl and η^3-benzyl coordination; examples of η^n-coordinated triarylmethyl complexes are $[(acac)M(\eta^3\text{-}CPh_3)]$ (M = Pd, Pt),[67] $[(\eta^5\text{-}CPh_3)(\eta^n\text{-}CPh_3)Yb(THF)_2]$ (*n* = 1–2)[68] and $[\{\kappa^4 COO'O''\text{-}C(C_6H_2{}^t Bu_2O\text{-}o)_3\}Zr(THF)_3]$.[69] The η^2*BC*-coordination mode in **5** provides a link between the η^1*B*- and η^3*BCC*-bonding extremes, much as η^2-benzyl coordination lies intermediate between the η^1- and η^3-benzyl coordination modes. For comparison, M–B bond distances of 2.320, 2.297 and 2.63 Å, and M–C_{ipso} distances of 2.198, 2.019 and 2.33 Å were observed in the η^3-arylborane complexes [Pd(TXPB)], [Ni(TXPB)][3] and $[Cp(CO)Fe(\mu\text{-}CO)_2Rh(TXPB)]$,[4] respectively. However, the M–C_{ortho} distances of 2.325, 2.081 and 2.46 Å in these complexes are much shorter than the Rh–C_{ortho} distance in **5**.

An η^2*BC*-coordination mode has also been reported for the borataalkene complexes $[(CO)Cp_2Ta\{\eta^2\text{-}CH_2B(C_6F_5)_2\}]$[70] and $[({}^t BuNC)Cp_2Ta\{\eta^2\text{-}CH_2B(C_6F_5)_2\}]$,[71] with Ta–C bond distances of 2.337 and 2.348 Å, Ta–B bond distances of 2.728 and 2.738 Å, and B–C distances of 1.508 and 1.525

Å, respectively. However, the B–C distance of 1.576(4) Å in **5** is in the usual range for a B–C_{sp2} single bond (e.g. 1.571–1.589 Å in BPh_3),[72] and C–C distances in the coordinated *B*–phenyl ring are not obviously perturbed from typical values. The η^2*BC*-interaction in complex **5** is therefore not significantly boratalkene-like, and presumably involves η^1-arene coordination and a dative η^1-borane interaction.

Based on this bonding description, the approximate planarity of the borane and the long Rh–B distance of 2.557(3) Å in **5** is not unusual; boron remains planar in the weakly coordinated η^1-borane complexes [ClAu{$P^iPr_2(C_6H_4)$BFlu-*o*}] ($\sum$(C-B-C) = 356°) and [ClAu{$P^iPr_2(C_6H_4)$BCy$_2$-*o*}] ($\sum$(C-B-C) = 359°),[6] which also exhibit long Au–B distances of 2.66 Å and 2.90 Å, respectively. The borane is also approximately planar in the η^3-coordinated arylborane complexes [Pd(TXPB)], [Ni(TXPB)] and [(TXPB)Rh(μ-CO)$_2$Fe(CO)Cp]. However, short metal–borane distances have been shown to be accessible in cationic ambiphilic ligand complexes; a somewhat shorter M–B distance was observed in cationic [({*o*-^{i}Pr$_2$P(C$_6$H$_4$)}$_3$B)Au][GaCl$_4$] (Au–B = 2.448 Å),[73] and substantially shorter M–B bonds were observed in the structurally rigid B(mt^R)$_3$ and B(taz)$_3$ complexes [Rh(CO)(PPh$_3$){B(taz)$_3$}][PF$_6$] (taz = 4-ethyl-3-methyl-5-thioxo-1,2,4-triazolyl) (Rh–B = 2.155 Å),[74] [Co(PPh$_3$){B(mt$^{t\text{Bu}}$)$_3$}][X] (X = BPh_4, PF_6, or SbF_6) (Co–B = 2.132 Å),[75] [Rh(CN^{t}Bu)(PPh$_3$){B(mt)$_3$}]Cl (Rh–B = 2.155 Å), [Rh(CNXyl)(PPh$_3$){B(mt)$_3$}]Cl (Rh–B = 2.146 Å), and [Rh(PMe$_3$)$_2$){B(mt)$_3$}]Cl (Rh–B = 2.148 and 2.153 Å).[76]

The CO stretching frequency for **5** is 2028 cm^{-1} in Nujol and 2038 cm^{-1} in CH_2Cl_2. These values are much higher than those for complexes **1–4**, indicating significantly reduced electron density at the rhodium centre. The difference in ν(CO) between zwitterionic **4** and cationic **5** can be attributed in large part to more effective electron donation from the TXPB–F ligand in **4,** relative to the TXPB ligand in **5**. This may be explained in terms of the formal negative charge on the TXPB–F ligand, combined with different arylborate/arylborane binding modes; η^2-arene binding in **4** versus η^2*BC*-arylborane coordination in **5**. However, increasing positive charge at a carbonyl ligated metal centre has been shown to reduce the extent to which the bonding orbitals of CO are polarized towards oxygen, resulting

in enhanced covalency and an increase in the CO stretching force constant.[77] A portion of the increase in ν(CO) from **4** to **5** may therefore arise from polarization effects due to the overall positive charge on complex **5**, rather than a decrease in the extent of π-backdonation.

Summary and Conclusions:

A series of ambiphilic ligand rhodium(I) halide complexes, [RhX(CO)(TXPB)] [X = Cl (**1**), Br (**2**), I (**3**) and F (**4**); TXPB = a phosphine-thioether-borane ligand], have been prepared, as well as the halide-free cation [Rh(CO)(TXPB)][PF_6] (**5**). Complex **1** was accessed via reaction of TXPB with [{Rh(μ-Cl)$(CO)_2$}$_2$] and was used as the starting material for the preparation of complexes **2–5**, either by halide substitution or halide abstraction. In all complexes, the TXPB ligand binds to rhodium via the phosphine and thioether groups, as well as an additional Rh–X–B, Rh–(η^2*CC*-Ar_3BF) or Rh–(η^2*BC*-BAr_3) interaction. In complex **3**, the iodide proved to form a strong bonding interaction with rhodium, but only a weak interaction with the borane in TXPB due to the incompatibility of a hard borane Lewis acid with a soft iodide ligand. By contrast, the bromide and chloride ligands in **1** and **2** adopt bridging positions between rhodium and boron, with a stronger halide–boron interaction in the chloro complex. Bridging chloride interactions between a metal and a Lewis acidic borane are rare, and to the best of our knowledge, complex **2** is the first example of a bridging metal–bromide–borane interaction. In the case of complex **4**, fluoride binds to the borane to form an anionic TXPB–F ligand, and the complex exhibits a weak 6.2 Hz $J_{P,F}$ coupling in the room temperature ^{31}P NMR spectrum. In contrast to zwitterionic **4**, the metal centre in cationic **5** engages in η^2*BC*-coordination of the borane in TXPB. The metal–boron interaction in this complex is weak, based on an ^{11}B NMR chemical shift of 57 ppm, which combined with an overall positive charge on the complex, and less effective electron-donation from neutral TXPB (relative to the anionic TXPB–F ligand in **4**), leads to a carbonyl stretching frequency shifted 20-25 cm^{-1} to higher frequency of that in **4**.

Based on these crystallographic and spectroscopic data, it may be concluded that Rh–X coordination becomes increasingly favorable, relative to B–X bond formation, as group 17 is descended, consistent with the predictions of hard-soft acid-base theory.[78] However in this system, a significant M–X–B bridging interaction *is* maintained for bromide, and a weak interaction persists even in the case of iodide. Nonetheless, iodide is by a wide margin the most suitable choice for the preparation of halide-containing ambiphilic ligand complexes in which a free pendant borane is required for cooperative reactivity. These results also confirm that in principle, it should be possible to use ambiphilic borane-containing ligands to provide an additional thermodynamic driving force for oxidative addition of less reactive aryl-chloride and aryl-fluoride substrates; either by the formation of a bridging M–Cl–BR_3 interaction or by fluoride abstraction to yield an anionic fluoroborate and a cationic metal centre. However, preliminary reactions (stoichiometric and catalytic conditions) of previously reported [Pd(TXPB)][3] with aryl chloride and aryl fluoride substrates have so far proved unsuccessful. This is perhaps unsurprising given the nature of the donor atoms in TXPB, and current efforts are focused on more electron-donating and thioether-free ambiphilic ligands likely to result in group 10 metal complexes with higher inherent activities for Ar–X oxidative addition and C–C bond forming catalysis.

Experimental:

General Details. An argon-filled MBraun UNIlab glovebox equipped with a –30°C freezer was employed for the manipulation and storage of all ligands and complexes, and reactions were performed on a double-manifold high vacuum line using standard techniques.[79] Commonly utilized specialty glassware includes the swivel frit assembly, J-Young NMR tubes, and thick-walled flasks equipped with Teflon stopcocks. A Fisher Scientific Ultrasonic FS-30 bath and a Branson 2510 Ultrasonic bath was used to sonicate reaction mixtures where indicated, and in some cases, a Fischer Scientific Model 228 centrific centrifuge in combination with airtight Kimble-Kontes 15 mL conical centrifuge tubes was used to remove insoluble byproduct or to collect precipitated products. Residual oxygen and moisture

were removed from the argon stream by passage through an Oxisorb-W scrubber from Matheson Gas Products.

Anhydrous CH_2Cl_2 was purchased from Aldrich. Hexanes and toluene were initially dried and distilled at atmospheric pressure from CaH_2 and sodium, respectively. Unless otherwise noted, all proteo solvents were stored over an appropriate drying agent (dme, toluene = Na/Ph_2CO; hexanes = Na/Ph_2CO/tetraglyme; CH_2Cl_2 = CaH_2) and introduced to reactions via vacuum transfer with condensation at −78°C. Deuterated solvents (ACP Chemicals) were dried over CaH_2 (CD_2Cl_2) or Na/Ph_2CO (C_6D_6). [{Rh(μ-Cl)$(CO)_2$}$_2$], Me_3SiBr, Me_3SiI, [NMe_4]F, and Tl[PF_6] were purchased from Sigma-Aldrich and stored under argon. Prior to use, [NMe_4]F was heated to 120°C for 3 days under dynamic vacuum. The TXPB ligand,[2] [RhCl(CO)(TXPB)] (**1**),[4] $Cl_2P(NEt_2)$[80] and $ClP(C_6D_5)_2$[81] were prepared according to literature procedures. The d_{10}-TXPB ligand and ***d*$_{10}$-1** were prepared using procedures identical to those for TXPB and **1**, but using $ClP(C_6D_5)_2$ and d_{10}-TXPB, respectively

IR Spectra were recorded on a Thermo Scientific Nicolet 6700 FTIR spectrometer. Combustion elemental analyses were performed on a Thermo EA1112 CHNS/O analyzer by Dr. Steve Kornic of this department. NMR spectroscopy (^{1}H, ^{13}C{^{1}H}, ^{11}B, ^{19}F, ^{31}P, DEPT-135, COSY, TOCSY, HSQC, HMBC) was performed on Bruker DRX-500 and AV-600 spectrometers. All ^{1}H NMR and ^{13}C NMR spectra were referenced relative to $SiMe_4$ through a resonance of the employed deuterated solvent or proteo impurity of the solvent; C_6D_6 (7.16 ppm) and CD_2Cl_2 (5.32 ppm) for ^{1}H NMR; C_6D_6 (128.0 ppm) and CD_2Cl_2 (54.0 ppm) for ^{13}C NMR. ^{11}B, ^{31}P, and ^{19}F NMR spectra were referenced using an external standard of $BF_3(OEt_2)$ (0.0 ppm), 85% H_3PO_4 in D_2O (0.0 ppm), and $CFCl_3$ (0.0 ppm), respectively. Temperature calibration was performed using a d_4-methanol sample, as outlined in the Bruker VTU user manual.[82] Values of $\Delta G^{\ddagger}$ for C*Me*$_2$ methyl group exchange were calculated using the equation $\Delta G^{\ddagger}$ (kJ mol^{-1}) = $-RT_c \ln[(\pi h \delta\nu)/(2^{1/2} k_B T_c)] = RT_c [22.96 + \ln(T_c / \delta\nu)]$ where R is the ideal gas constant, h is Planck's constant, and k_B is the Boltzmann constant.[86] The values of δν (NMR frequency difference in Hz) and T_c (coalescence temperature) used were 364.8 Hz and 254 K for **1**, 290.4 Hz and 211 K for **2**, 278.0 Hz and 210 K for **3**, 384.6 Hz and 274 K for **4**, and 165.0 Hz and 312 K for **5**. Herein, numbered

proton and carbon atoms refer to the positions of the xanthene backbone in the TXPB ligand (see Scheme 1).

X-ray crystallographic analyses were performed on suitable crystals coated in Paratone oil and mounted on a SMART APEX II diffractometer with a 3 kW Sealed tube Mo generator in the McMaster Analytical X-Ray (MAX) Diffraction Facility. One of two molecules of hexane within the asymmetric unit cell of **2**·hexane, one molecule of hexane in **3**·hexane, and a half molecule of CH_2Cl_2 in **4**·1.5CH_2Cl_2 were highly disordered and could not be modeled satisfactorily, so were treated using the SQUEEZE routine.[87] In addition, the following groups were rotationally or positionally disordered over two positions: (a) both of the *tert*-butyl substituents for molecule B in **2**·hexane, (b) one of the *tert*-butyl substituents in **4**·1.5CH_2Cl_2, (c) one molecule of CH_2Cl_2 in **4**·1.5CH_2Cl_2, and (d) the PF_6 anion in **5**·CH_2Cl_2. In all cases, disorder was modeled allowing occupancy and positional parameters to refine freely. All *tert*-butyl methyl groups (cases a and b above) were restrained to have equivalent thermal parameters. However, (a) was refined isotropically while (b) was refined anisotropically. For case (c), carbon and chlorine atoms were restrained to have equivalent thermal parameters, respectively, and were refined anisotropically. For case (d), all fluorine atoms were restrained to have similar thermal parameters using the SIMU command, and refinements were performed using the ISOR command.

[RhBr(CO)(TXPB)]·hexane (2): Me_3SiBr (25 μL, 1.90 × 10^{-4} mol) was added dropwise at room temperature to [RhCl(CO)(TXPB)] (160 mg, 1.88 × 10^{-4} mol) in CH_2Cl_2 (10 ml). The reaction mixture was stirred vigorously for 2 hours at room temperature before evaporation to dryness *in vacuo*. The resulting tangerine-coloured powder was left under dynamic vacuum for 3 hours to ensure removal of all solvent and Me_3SiCl. Further purification entailed washing with hexanes (×2) with cooling to –30°C for 1 hour before decanting the mother liquors during each washing, and subsequent drying *in vacuo.* Yield = 125 mg (74%). X-ray quality crystals of **2**·hexane were grown by cooling a saturated solution of **2** in hexanes to –30°C for several days. **^{1}H NMR (CD_2Cl_2, 20°C):** δ 7.78 (d, $^4J_{H,H}$ 2 Hz, 1H, C*H*^{1}), 7.63 (d, $^4J_{H,H}$ 2 Hz, 1H, C*H*^{8}), 7.47 (tt, $^3J_{H,H}$ 7, $^4J_{H,H}$ 1.8 Hz, 2H, *p*-P*Ph*$_2$), 7.41 – 7.33 (m, 8H, *o* + *m*-P*Ph*$_2$), 7.32 (dd, $^3J_{H,H}$ 8, $^4J_{H,H}$ 1 Hz, 4H, *o*-B*Ph*$_2$), 7.28 (dd, $^3J_{H,P}$ 9, $^4J_{H,H}$ 2 Hz, 1H, C*H*^{3}), 7.07 (app t, $^3J_{H,H}$ 7 Hz, 4H,

m-B*Ph*$_2$), 7.02 (d, $^4J_{H,H}$ 2 Hz, 1H, C*H*^{6}), 7.00 (t, $^3J_{H,H}$ 7 Hz, 2H, *p*-B*Ph*$_2$), 1.86 (s, 6H, C*Me*$_2$), 1.25, 1.15 (s, 2 x 9H, C*Me*$_3$). **^{13}C{^{1}H} NMR (CD_2Cl_2, 20°C):** δ 187.6 (dd, $^1J_{C,Rh}$ 77, $^2J_{C,P}$ 15 Hz, Rh*C*O), 153.1 (d, $^3J_{C,P}$ 6 Hz, *C*^{2}CMe$_3$), 150.0 (s, *C*^{7}CMe$_3$), 148.5 (broad s, *ipso*-B*Ph*$_2$), 148.0 (broad s, *C*^{5}), 146.0 (d, $^3J_{C,P}$ 14 Hz, *C*^{10}), 142.2 (s, *C*^{13}), 137.3 (d, $^2J_{C,P}$ 27 Hz, *C*^{11}), 136.5 (s, *o*-B*Ph*$_2$), 133.8 (d, $^1J_{C,P}$ 50 Hz, *C*^{4}), 133.7 (d, $^2J_{C,P}$ 12 Hz, *o*-P*Ph*$_2$), 133.5 (s, *C*^{6}), 133.0 (d, $^1J_{C,P}$ 55 Hz, *ipso*-P*Ph*$_2$), 131.6 (s, *p*-P*Ph*$_2$), 130.2 (s, *C*^{12}), 129.1 (d, $^3J_{C,P}$ 11 Hz, *m*-P*Ph*$_2$), 128.4 (s, *C*^{3}), 127.4 (s, *p*-B*Ph*$_2$), 127.0 (*m*-B*Ph*$_2$), 125.8 (s, *C*^{1}), 122.2 (s, *C*^{8}), 42.9 (s, *C*Me$_2$), 35.6, 35.2 (s, 2 x *C*Me$_3$), 31.5 (s, 2 x C*Me*$_3$), 26.7 (s, C*Me*$_2$). **^{31}P {^{1}H} (CD_2Cl_2, 20°C):** δ +64.5 (d, $^1J_{P,Rh}$ 164 Hz). **^{11}B (CD_2Cl_2, 20°C):** δ +27 (v.broad s, $\omega_{1/2} \approx$ 900 Hz). **IR:** ν(CO) = 2013 cm^{-1} (nujol), 2008 cm^{-1} (CH_2Cl_2). **Anal.** Calcd. For $C_{54}H_{62}OBrPSBRh$: C, 65.93; H, 6.35. Found: C, 66.17; H, 5.91%.

[RhI(CO)(TXPB)]·0.5hexane (3): A solution of Me_3SiI (48.1 mg, 2.40×10^{-4} mol) in CH_2Cl_2 (2 ml) was added dropwise at room temperature to [RhCl(CO)(TXPB)] (205 mg, 2.40×10^{-4} mol) in CH_2Cl_2 (10 ml). The reaction mixture was stirred vigorously for 1 hour before evaporation to dryness *in vacuo*. The resulting rust–red powder was left under dynamic vacuum for 3 hours to ensure all solvent and Me_3SiCl had been removed. Further purification entailed washing with hexanes (×2) with cooling to –30°C for 1 hour before decanting the mother liquors during each washing, and subsequent drying *in vacuo*. Yield = 187 mg (83%). X-ray quality crystals of **3**·hexane were grown by cooling a saturated solution of **3** in hexanes to –30°C for several days. **^{1}H NMR (C_6D_6, 20°C):** δ 7.83 (d, $^3J_{H,H}$ 7 Hz, 4H, *o*-B*Ph*$_2$), 7.80 (s, 1H, C*H*^{8}), 7.69 (s, 1H, C*H*^{1}), 7.56 (d, $^3J_{H,P}$ 8 Hz, 1H, C*H*^{3}), 7.48-7.41 (m, 5H, C*H*^{6} + *o*-P*Ph*$_2$), 6.95 (t, $^3J_{H,H}$ 7 Hz, 2H, *p*-P*Ph*$_2$), 6.92-6.83 (m, 8H, *m*-P*Ph*$_2$ + *m*-B*Ph*$_2$), 6.76 (t, $^3J_{H,H}$ 6 Hz, 2H, *p*-B*Ph*$_2$), 1.73 (s, 6H, C*Me*$_2$), 1.18, 1.10 (s, 2 x 9H, C*Me*$_3$). **^{13}C{^{1}H} NMR (C_6D_6, 20°C):** δ 189.7 (dd, $^1J_{C,Rh}$ 74, $^3J_{C,P}$ 14 Hz, Rh*C*O), 152.5 (d, $^3J_{C,P}$ 5 Hz, *C*^{2}CMe$_3$), 149.7 (s, *C*^{7}CMe$_3$), 147.6 (broad s, *C*^{5}), 146.9 (d, $^3J_{C,P}$ 14 Hz, *C*^{10}), 143.8 (broad s, *ipso*-B*Ph*$_2$), 143.7 (s, *C*^{13}), 140.4 (d, $^2J_{C,P}$ 32 Hz, *C*^{11}), 139.1 (s, *o*-B*Ph*$_2$), 134.2 (s, *C*^{6}), 134.1 (d, $^1J_{C,P}$ 51 Hz, *ipso*-P*Ph*$_2$), 133.4 (d, $^2J_{C,P}$ 12 Hz, *o*-P*Ph*$_2$), 133.1 (s, *C*^{4}), 132.4 (s, *C*^{12}), 130.5 (s, *p*-P*Ph*$_2$), 129.0 (s, *p*-B*Ph*$_2$), 128.5 (d, $^3J_{C,P}$ 11 Hz, *m*-P*Ph*$_2$), 128.3 (s, *C*^{3}), 126.8 (s, *m*-B*Ph*$_2$), 125.1 (s, *C*^{1}), 123.1 (s, *C*^{8}), 43.3 (s, *C*Me$_2$), 35.1, 35.0 (s, 2 x *C*Me$_3$), 31.4, 31.3 (s, 2

x C*Me*$_3$), 26.1 (s, C*Me*$_2$). **^{31}P {^{1}H} (CD_2Cl_2, 20°C):** δ +67.2 (d, $^1J_{P,Rh}$ 167 Hz). **^{11}B (CD_2Cl_2, 20°C):** δ +56 (v.broad s, $\omega_{1/2} \approx$ 1800 Hz). **IR:** ν(CO) = 2004 cm^{-1} (Nujol), 2002 cm^{-1} (CH_2Cl_2). **Anal.** Calcd. For $C_{51}H_{55}OBrPSBRh$: C, 62.02; H, 5.61. Found: C, 61.95; H, 5.79%.

[Rh(CO)(TXPB-F)] (4): A mixture of [RhCl(CO)(TXPB)] (50 mg, 5.86×10^{-5} mol) and [NMe_4]F (5.5 mg, 5.91×10^{-5} mol) in CH_2Cl_2 (5 ml) was stirred vigorously for 1 hour at room temperature. The resulting orange, opaque mixture was filtered through a column of celite, and the red / orange mother liquors were evaporated to dryness *in vacuo* to yield a rust-red powder. Yield = 35 mg (72 %). X-ray quality crystals of **4**·1.5CH_2Cl_2 were grown by slow diffusion of hexanes into a solution of **4** in CH_2Cl_2 at –30°C. **^{1}H NMR (CD_2Cl_2, –50°C):** δ 7.68 (s, 2H, C*H*^{1}), 7.66 (m, 2H, *o*-P*Ph*$_2$ A), 7.59 (broad s, 3H, *p*-P*Ph*$_2$ A + *o*-B*Ph*$_2$ A), 7.55 (t, 2H, *o*-P*Ph*$_2$ A), 7.48–7.41 (m, 3H, *p*-P*Ph*$_2$ B + *m*-B*Ph*$_2$ A), 7.39 (s, 1H, C*H*^{8}), 7.34 (broad s, 2H, *m*-P*Ph*$_2$ B), 7.25 (m, 2H, *o*-P*Ph*$_2$ B), 7.21 (t, $^3J_{H,H}$ 7 Hz, 1H, *p*-B*Ph*$_2$ A), 7.13 (app t, $^3J_{H,H}$ 7 Hz, 2H, *m*-B*Ph*$_2$ B), 7.03 (s, 1H, C*H*^{6}), 7.01 (t, 1H, *p*-B*Ph*$_2$ B), 6.96 (broad s, 2H, *o*-B*Ph*$_2$ B), 6.91 (d, $^3J_{H,P}$ 11 Hz, 1H, C*H*^{3}), 2.03, 1.26 (s, 2 x 3H, C*Me*$_2$), 1.16, 1.13 (s, 9H, 2 x C*Me*$_3$). **^{13}C{^{1}H} NMR (CD_2Cl_2, –50°C):** δ 186.8 (dd, $^1J_{C,Rh}$ 75, $^3J_{C,P}$ 19 Hz, Rh*C*O), 151.9 (d, $^3J_{C,P}$ 7 Hz, *C*^{2}CMe$_3$), 149.5 (s, *C*^{7}CMe$_3$), 141.1 (d, $^3J_{C,P}$ 14 Hz, *C*^{10}), 138.1 (s, *C*^{13}), 135.7 (d, $^2J_{C,P}$ 23 Hz, *C*^{11}), 134.3 (d, $^1J_{C,P}$ 53 Hz, C^4), 133.6 (d, $^3J_{C,P}$ 12 Hz, *m*-P*Ph*$_2$ A), 133.1 (broad s, *ipso*-B*Ph*$_2$ A), 132.6 (d, $^2J_{C,P}$ 12 Hz, *o*-P*Ph*$_2$ B), 131.9 (s, *p*-P*Ph*$_2$ A), 131.7 (s, *o*-B*Ph*$_2$ A + *o*-B*Ph*$_2$ B + *p*-P*Ph*$_2$ B), 131.5 (app s, *ipso*-P*Ph*$_2$ A + *ipso*-B*Ph*$_2$ B), 131.2 (d, $^1J_{C,P}$ 37 Hz, *ipso*-P*Ph*$_2$ B), 129.9 (broad s, C^6), 129.4 (d, $^2J_{C,P}$ 12 Hz, *m*-P*Ph*$_2$ A), 129.2 (s, *m*-B*Ph*$_2$ A), 128.8 (d, $^3J_{C,P}$ 12 Hz, *m*-P*Ph*$_2$ B), 128.6 (s, *p*-B*Ph*$_2$ A), 128.1 (broad s, C^5), 127.6 (s, C^3), 127.2 (s, *m*-B*Ph*$_2$ B), 126.2 (s, C^{12}), 125.4 (s, *C*^{1}), 125.1 (s, *p*-B*Ph*$_2$ B), 119.7 (s, *C*^{8}), 40.7 (s, *C*Me$_2$), 35.1, 34.8 (s, 2 x *C*Me$_3$), 31.2, 30.8 (s, 2 x C*Me*$_3$), 27.8, 24.9 (s, 2 x C*Me*$_2$). **^{31}P {^{1}H} (CD_2Cl_2, 20°C):** δ +52.2 (dd, $^1J_{P,Rh}$ 166, $J_{P,F}$ 6.2 Hz). **^{19}F (CD_2Cl_2, 20°C):** δ -186 (broad s, $\omega_{1/2} \approx$ 180 Hz). **^{11}B (CD_2Cl_2, 20°C):** δ +4 (broad s, $\omega_{1/2} \approx$ 350 Hz). **IR:** ν(CO) = 2008 cm^{-1} (Nujol), 2011 cm^{-1} (CH_2Cl_2). **Anal.** Calcd. For $C_{48}H_{48}OFPSBRh$: C, 68.91; H, 5.78. Found: C, 69.27; H, 5.60%.

[Rh(CO)(TXPB)][PF_6]·0.5CH_2Cl_2 (5): A mixture of [RhCl(CO)(TXPB)] (350 mg, 4.10×10^{-4} mol) and Tl[PF_6] (350 mg, 1.00×10^{-3} mol) in CH_2Cl_2 (10 ml) was stirred vigorously for 4.5 hours at room

temperature. After allowing any solid to settle over 24 hours at -30°C, the mother liquors were carefully decanted, layered with hexanes, and cooled to -30°C for several days. The resulting orange needles were washed with hexanes (×1) and dried *in vacuo*. Yield = 363 mg (92 %). X-ray quality crystals of **5**·CH_2Cl_2 were grown by slow diffusion of hexanes into a solution of **5** in CH_2Cl_2 at –30°C. **^{1}H NMR (CD_2Cl_2, –70 °C):** δ 8.27 (d, $^3J_{H,H}$ 7 Hz, 2H, *o*-B*Ph*$_2$ A), 8.08 (t, $^3J_{H,H}$ 7 Hz, 1H, *p*-B*Ph*$_2$ A), 7.81 (app t, $^3J_{H,H}$ 7 Hz, 2H, *m*-B*Ph*$_2$ A), 7.75 (s, 1H, C*H*^{1}), 7.71 (s, 1H, C*H*^{8}), 7.66 (t, $^3J_{H,H}$, 1H, *p*-B*Ph*$_2$ B), 7.60 (d, $^3J_{H,H}$ 7 Hz, 2H, *o*-B*Ph*$_2$ B), 7.56 (t, $^3J_{H,H}$ 8 Hz, 2H, 2 x *p*-P*Ph*$_2$), 7.54 (app t, $^3J_{H,H}$ 8 Hz, 2H, *m*-B*Ph*$_2$ B), 7.54-7.45 (m, 4H, *o*/*m*-P*Ph*$_2$), 7.38-7.30 (m, 4H, *o*/*m*-P*Ph*$_2$), 7.21 (s, 1H, C*H*^{6}), 7.13 (d, $^3J_{H,P}$ 10 Hz, 1H, C*H*^{3}), 2.13, 1.80 (s, 2 x 3H, C*Me*$_2$), 1.21, 1.14 (s, 9H, 2 x C*Me*$_3$). **^{13}C{^{1}H} NMR (CD_2Cl_2, –70 °C):** δ 183.3 (dd, $^1J_{C,Rh}$ 72, $^3J_{C,P}$ 13 Hz, Rh*C*O), 155.3 (s, *C*^{2}CMe$_3$), 152.0 (s, *C*^{7}CMe$_3$), 145.7 (d, $^3J_{C,P}$ 13 Hz, *C*^{10}), 144.5 (s, *C*^{12}), 142.3 (s, *C*^{13}), 139.8 (s, *p*-B*Ph*$_2$ A), 139.3 (broad s, *ipso*-B*Ph*$_2$ B), 137.4 (s, *o*-B*Ph*$_2$ B), 136.2 (s, *o*-B*Ph*$_2$ A), 135.9 (d, $^2J_{C,P}$ 24 Hz, *C*^{11}), 133.3 (d, *J* 12 Hz, *o*/*m*-P*Ph*$_2$), 133.0 (s, *C*^{6}), 132.8 (s, *p*-B*Ph*$_2$ B), 132.4 (s, 2 x *p*-P*Ph*$_2$), 132.3 (d, *J* 12 Hz, *o*/*m*-P*Ph*$_2$), 132.2 (s, *C*^{5}), 130.0 (d, $^1J_{C,P}$ ~ 60 Hz, *C*^{4} or *ipso*-P*Ph*$_2$), 129.7 (d, *J* 12 Hz, *o*/*m*-P*Ph*$_2$), 129.4 (s, *m*-B*Ph*$_2$ A), 129.0 (d, *J* 12 Hz, *o*/*m*-P*Ph*$_2$), 128.9 (d, $^1J_{C,P}$ 59 Hz, C^4 or *ipso*-P*Ph*$_2$), 128.3 (s, *m*-B*Ph*$_2$ B), 127.4 (s, *C*^{1}), 127.1 (s, *C*^{3}), 125.60 (s, *C*^{8}), 110.8 (broad s, *ipso*-B*Ph*$_2$ A), 43.3 (s, *C*Me$_2$), 35.2, 35.0 (s, 2 x *C*Me$_3$), 30.8, 30.6 (s, 2 x C*Me*$_3$), 26.4, 25.0 (s, 2 x C*Me*$_2$). **^{31}P{^{1}H} (CD_2Cl_2, 20 °C):** δ +64.9 (d, $^1J_{P,Rh}$ 166.8 Hz). **^{11}B (CD_2Cl_2, 20 °C):** δ +57 (broad s, $\omega_{1/2} \approx$ 1800 Hz). **IR:** ν(CO) = 2028 cm^{-1} (Nujol), 2038 cm^{-1} (CH_2Cl_2). **Anal.** Calcd. for $C_{48}H_{48}P_2SBF_6Rh$: C, 57.96; H, 4.91. Found: C, 57.73; H, 5.09 %.

Acknowledgements. D.J.H.E. thanks NSERC of Canada for a Discovery Grant, the Ontario Ministry of Resarch and Innovation for an Early Researcher Award, and Canada Foundation for Innovation (CFI) and Ontario Innovation Trust (OIT) for New Opportunities Grants. B.E.C. thanks the Government of Ontario for an Ontario Graduate Scholarship (OGS).

Supporting Information Available: X-ray crystallographic data in PDF format and CIF files are available free of charge *via* the internet at http://pubs.acs.org.

References

(1) (a) Braunschweig, H.; Kollann, C.; Rais, D. *Angew. Chem. Int. Ed. Engl.* **2006**, *45*, 5254. (b) Fontaine, F.-G.; Boudreau, J.; Thibault, M.-H. *Eur. J. Inorg. Chem.* **2008**, 5439.

(2) Emslie, D. J. H.; Blackwell, J. M.; Britten, J. F.; Harrington, L. E. *Organometallics* **2006**, *25*, 2412.

(3) Emslie, D. J. H.; Harrington, L. E.; Jenkins, H. A.; Robertson, C. M.; Britten, J. F. *Organometallics* **2008**, *27*, 5317.

(4) Oakley, S. R.; Parker, K. D.; Emslie, D. J. H.; Vargas-Baca, I.; Robertson, C. M.; Harrington, L. E.; Britten, J. F. *Organometallics* **2006**, *25*, 5835.

(5) Vergnaud, J.; Ayed, T.; Hussein, K.; Vendier, L.; Grellier, M.; Bouhadir, G.; Barthelat, J.-C.; Sabo-Etienne, S.; Bourissou, D. *Dalton Trans.* **2007**, 2370.

(6) Bontemps, S.; Bouhadir, G.; Miqueu, K.; Bourissou, D. *J. Am. Chem. Soc.* **2006**, *128*, 12056.

(7) Bontemps, S.; Bouhadir, G.; Aperley, D. C.; Dyer, P. W.; Miqueu, K.; Bourissou, D. *Chem. Asian J.* **2009**, *4*, 428.

(8) Lancaster, S. J.; Al-Benna, S.; Thornton-Pett, M.; Bochmann, M. *Organometallics* **2000**, *19*, 1599.

(9) Crevier, T. J.; Bennett, B. K.; Soper, J. D.; Bowman, J. A.; Dehestani, A.; Hrovat, D. A.; Lovell, S.; Kaminsky, W.; Mayer, J. M. *J. Am. Chem. Soc.* **2001**, *123*, 1059.

(10) Languérand, A.; Barnes, S. S.; Bélanger-Chabot, G.; Maron, L.; Berrouard, P.; Audet, P.; Fontaine, F.-G. *Angew. Chem. Int. Ed. Engl.* **2009**, *48*, 6695.

(11) Antiñolo, A. C.-H., F.; Fernández-Baeza, J.; García-Yuste, S.; Otero, A.; Sánchez-Prada, J.; Villaseñor, E. *J. Organomet. Chem.* **2000**, *609*, 123.

(12) For recent examples of complexes featuring M-F-BF_3 bridging interactions, see: (a) Frech, C. M.; Shimon, L. J. W.; Milstein, D. *Organometallics* **2009**, *28*, 1900. (b) Tkach, V. S.; Myagmarsuren, G.; Suslov, D. S.; Darjaa, T.; Dorj, D.; Shmidt, F. K. *Cat. Comm.* **2008**, *9*, 1501. (c) Majumdar, M.; Patra, S. K.; Kannan, M.; Dunbar, K. R.; Bera, J. K. *Inorg. Chem.* **2008**, *47*, 2212. (d) Feller, M.; Ben-Ari, E.; Gupta, T.; Shimon, L. J. W.; Leitus, G.; Diskin-Posner, Y.; Weiner, L.; Milstein, D. *Inorg. Chem.* **2007**, *46*, 10479. (e) Drabent, K.; Clunlk, Z.; Ozarowskl, A. *Inorg. Chem.* **2008**, *47*, 3358.

(13) (a) Pang, K.; Tanski, J. M.; Parkin, G. *Chem. Commun.* **2008**, 1008. (b) Figueroa, J. S.; Melnick, J. G.; Parkin, G. *Inorg. Chem.* **2006**, *45*, 7056.

(14) Fischer, E. O.; Bock, M. *J. Organomet. Chem.* **1985**, *287*, 279.

(15) (a) Kiplinger, J. L.; Richmond, T. G.; Osterberg, C. E. *Chem. Rev.* **1994**, *94*, 373. (b) Grushin, V. V.; Alper, H. *Chem. Rev.* **1994**, *94*, 1047. (c) Torrens, H. *Coord. Chem. Rev.* **2005**, *249*, 1957. (d) Murphy, E. F.; Murugavel, R.; Roesky, H. W. *Chem. Rev.* **1997**, *97*, 3425. (e) Amii, H.; Uneyama, K. *Chem. Rev.* **2009**, *109*, 2119. (f) Perutz, R. N.; Braun, T., Chapter 1.26: Transition Metal-mediated C-F Bond Activation. In *Comprehensive Organometallic Chemistry III*, Parkin, G., Ed.; Elsevier Ltd.: Oxford, 2007; Vol. 3. Compounds of Groups 13-15, p 725. (g) For a recent example of aryl-fluoride reductive elimination from palladium(II), see: Watson, D. A.; Su, M.; Teverovskiy, G.; Zhang, Y.; García-Fortanet, J.; Kinzel, T.; Buchwald, S. L. *Science* **2009**, *325*, 1661.

(16) Burdeniuc, J.; Jedlicka, B.; Crabtree, R. H. *Chem. Ber.* **1997**, *130*, 145.

(17) Doherty, N. M.; Hoffman, N. W. *Chem. Rev.* **1991**, *91*, 553.

(18) In addition to thermodynamic challenges associated with C–F bond oxidative addition, theoretical studies have in several cases identified substantial kinetic barriers for this process (see refs 15a-e and 16). Recently, phosphine-assisted aryl fluoride oxidative addition has been reported as an alternative pathway for C–F bond activation, involving a four-centred transition state containing the metal, *ipso*-carbon, fluorine and phosphorus atoms (see ref 19). The borane

group of an ambiphilic ligand could in principle assume a similar role [differing in the absence of a metal–ER_3 (E = B or P) interaction], also leading to reduced kinetic barriers for Ar–F oxidative addition.

(19) (a) Nova, A.; Erhardt, S.; Jasmin, N. A.; Perutz, R. N.; Macgregor, S. A.; McGrady, J. E.; Whitwood, A. C. *J. Am. Chem. Soc.* **2008**, *130*, 15499. (b) Erhardt, S.; Macgregor, S. A. *J. Am. Chem. Soc.* **2008**, *130*, 15490.

(20) (a) Labinger, J. A.; Miller, J. S. *J. Am. Chem. Soc.* **1982**, *104*, 6856. (b) Grimmett, D. L.; Labinger, J. A.; Bonfiglio, J. N.; Masuo, S. T.; Shearin, E.; Miller, J. S. *Organometallics* **1983**, *2*, 1325. (c) Labinger, J. A.; Bonfiglio, J. N.; Grimmett, D. L.; Masuo, S. T.; Shearin, E.; Miller, J. S. *Organometallics* **1983**, *2*, 733.

(21) (a) Fontaine, F.-G.; Zargarian, D. *J. Am. Chem. Soc.* **2004**, *126*, 8786. (b) Thibault, M. H.; Boudreau, J.; Mathiotte, S.; Drouin, F.; Sigouin, O.; Michaud, A.; Fontaine, F. G. *Organometallics* **2007**, *26*, 3807.

(22) (a) Crossley, I. R.; Hill, A. F.; Willis, A. C. *Organometallics* **2007**, *26*, 3891. (b) Fischbach, A.; Bazinet, P. R.; Waterman, R.; Tilley, T. D. *Organometallics* **2008**, *27*, 1135.

(23) (a) Baker, M. J.; Giles, M. F.; Orpen, A. G.; Taylor, M. J.; Watt, R. J. *J. Chem. Soc., Chem. Commun.* **1995**, 197. (b) Steeg, N.; Kramolowsky, R. *Z. Kristallogr. - New Cryst. Struct.* **1997**, *212*, 273. (c) Raghuraman, K.; Krishnamurthy, S. S.; Nethaji, M. *J. Organomet. Chem.* **2003**, *669*, 79.

(24) Brauer, D. J.; Bürger, H.; Chebude, Y.; Pawelke, G. *Inorg. Chem.* **1999**, *38*, 3972.

(25) (a) Cross, W. I.; Lightfoot, M. P.; Mair, F. S.; Pritchard, R. G. *Inorg. Chem.* **2000**, *39*, 2690. (b) Narula, C. K.; Nöth, H. *Inorg. Chem.* **1984**, *24*, 2532.

(26) Gunther, H., *NMR Spectroscopy*, Thieme Verlag: Stuttgart, 1992.

(27) Weller, F.; Mohlen, M.; Dehnicke, K. *Z. Kristallogr. - New Cryst. Struct.* **1997**, *212*, 159.

(28) Lijima, K.; Oonishi, I.; Shibata, S. *Chem. Lett.* **1983**, 251.

(29) Brown, D. S.; Carmalt, C. J.; Cowley, A. H.; Decken, A.; Isom, H. S. *Heteroatom Chem.* **1998**, *9*, 79.

(30) Steyl, G.; Kirsten, L.; Muller, A.; Roodt, A. *Acta Cryst.* **2006**, *E62*, m1127.

(31) Thomas, C. M.; Peters, J. C. *Inorg. Chem.* **2004**, *43*, 8.

(32) César, V.; Bellemin-Laponnaz, S.; Gade, L. H. *Eur. J. Inorg. Chem.* **2004**, 3436.

(33) Willems, S. T. H.; Budzelaar, P. H. M.; Moonen, N. N. P.; Gelder, R. D.; Smits, J. M. M.; Gal, A. W. *Chem. Eur. J.* **2002**, *8*, 1310.

(34) Kranich, R.; Eis, K.; Geis, O.; Mühle, S.; Bats, J. W.; Schmalz, H.-G. *Chem. Eur. J* **2000**, *6*, 2874.

(35) Dilworth, J. R.; W, C. A. M. v. B.; Pascu, S. I. *Dalton Trans.* **2005**, 2151.

(36) Cordero, B.; Gómez, V.; Platero-Prats, A. E.; Revés, M.; Echeverría, J.; Cremades, E.; Barragán, F.; Alvarez, S. *Dalton Trans.* **2008**, 2832.

(37) Aarset, K.; Shen, Q.; Thomassen, H.; Richardson, A. D.; Hedberg, K. *J. Phys. Chem. A* **1999**, *103*, 1644.

(38) Housecroft, C. E.; Sharpe, A. G., *Inorganic Chemistry*, 2nd ed.; Pearson Education Limited: London, 2005.

(39) Brunner, H.; Zettler, C.; Zabel, M. *Z. Anorg. Allg. Chem.* **2003**, *629*, 1131.

(40) Lamb, G.; Clarke, M.; Slawin, A. M. Z.; Williams, B.; Key, L. *Dalton Trans.* **2007**, 5582.

(41) Corey, E. J.; Rohde, J. J.; Fischer, A.; Mihai D, A. *Tetrahedron Lett.* **1997**, *38*, 33.

(42) Nie, Y.; Schwiegk, S.; Pritzkow, H.; Siebert, W. *Eur. J. Inorg. Chem.* **2004**, 1630.

(43) Black, D. L.; Taylor, R. C. *Acta Crystallogr. Sect. B-Struct. Commun.* **1975**, *31*, 1116.

(44) Jimenez-Rodriguez, C.; Pogorzelec, P. J.; Eastham, G. R.; Slawin, A. M. Z.; Cole-Hamilton, D. J. *Dalton Trans.* **2007**, 4160.

(45) Welch, G. C.; Cabrera, L.; Chase, P. A.; Hollink, E.; Masuda, J. D.; Wei, P.; Stephan, D. W. *Dalton Trans.* **2007**, 3407.

(46) Agou, T.; Kobayashi, J.; Kim, Y.; Gabbaï, F. P.; Kawashima, T. *Chem. Lett.* **2007**, *36*, 976.

(47) Yamaguchi, S.; Akiyama, S.; Tamao, K. *J. Am. Chem. Soc.* **2001**, *123*, 11372.

(48) Hannant, M. H.; Wright, J. A.; Lancaster, S. J.; Hughes, D. L.; Horton, P. N.; Bochmann, M. *Dalton Trans.* **2006**, 2415.

(49) Chiu, C.-W.; Gabbaï, F. P. *J. Am. Chem. Soc.* **2006**, *128*, 14248.

(50) Brauer, D. J.; Burger, H.; Hubinger, R.; Pawelke, G. *Z. Anorg. Allg. Chem.* **2001**, *627*, 679.

(51) (a) Bondi, A. *J. Phys. Chem.* **1964**, *68*, 441. (b) Nag, S.; Banerjee, K.; Datta, D. *New J. Chem.* **2007**, *31*, 832.

(52) Kuznetsov, V. F.; Facey, G. A.; Yap, G. P. A.; Alper, H. *Organometallics* **1999**, *18*, 4706.

(53) Zhao, P.; Incarvito, C. D.; Hartwig, J. F. *J. Am. Chem. Soc.* **2006**, *128*, 3124.

(54) (a) Grushin, V. V.; Marshall, W. J. *J. Am. Chem. Soc.* **2004**, *126*, 3068. (b) Macgregor, S. A.; Roe, D. C.; Marshall, W. J.; Bloch, K. M.; Bakhmutov, V. I.; Grushin, V. V. *J. Am. Chem. Soc.* **2005**, *127*, 15304. (c) Marshall, W. J.; Aullón, G.; Alvarez, S.; Dobbs, K. D.; Grushin, V. V. *Eur. J. Inorg. Chem.* **2006**, 3340.

(55) Mallory, F. B.; Mallory, C. W., *An Encyclopedia of Nuclear Magnetic Resonance*, Wiley: Chichester, 1996.

(56) Hierso, J.-C.; Fihri, A.; Ivanov, V. V.; Hanquet, B.; Pirio, N.; Donnadieu, B.; Rebière, B.; Amardeil, R.; Meunier, P. *J. Am. Chem. Soc.* **2004**, *126*, 11077.

(57) Thomas, D. A.; Ivanov, V. V.; Butler, I. R.; Horton, P. N.; Meunier, P.; Hierso, J.-C. *Inorg. Chem.* **2008**, *47*, 1607.

(58) Arnold, W. D.; Mao, J.; Sun, H.; Oldfield, E. *J. Am. Chem. Soc.* **2000**, *122*, 12164.

(59) CF_3 rotation averaged $J_{P,F}$ values were calculated as a function of P•••C distance. This was converted to a closest-approach P•••F distance by subtraction of 1.32 Å (the C–F distance in CF_4).

(60) Kruck, M.; Munoz, M. P.; Bishop, H. L.; Frost, C. G.; Chapman, C. J.; Kociok-Köhn, G.; Butts, C. P.; Lloyd-Jones, G. C. *Chem. Eur. J.* **2008**, *14*, 7808.

(61) Tuttle, T.; Gräfenstein, J.; Cremer, D. *Chem. Phys. Lett.* **2004**, *394*, 5.

(62) Miller, G. R.; Yankowsky, A. W.; Grim, S. O. *J. Chem. Phys.* **1969**, *51*, 3185.

(63) Jonáš, J.; Gutowsky, H. S. *J. Chem. Phys.* **1965**, *42*, 140.

(64) Iwaoka, M.; Komatsu, H.; Katsuda, T.; Tomoda, S. *J. Am. Chem. Soc.* **2002**, *124*, 1902.

(65) Benson, J. W. *Organometallics* **1998**, *17*, 4275.

(66) Thomas, J. C.; Peters, J. C. *Inorg. Chem.* **2003**, *42*, 5055.

(67) Sonoda, A.; Bailey, P. M.; Maitlis, P. M. *J. Chem. Soc., Dalton Trans.* **1979**, 346.

(68) Hitchcock, P. B.; Khvostov, A. V.; Lappert, M. F.; Protchenko, A. V. *Dalton Trans.* **2009**, 2383.

(69) Akagi, F.; Matsuo, T.; Kawaguchi, H. *J. Am. Chem. Soc.* **2005**, *127*, 11936.

(70) Cook, K. S.; Piers, W. E.; Woo, T. K.; McDonald, R. *Organometallics* **2001**, *20*, 3927.

(71) Cook, K. S.; Piers, W. E.; Rettig, S. J. *Organometallics* **1999**, *18*, 1575.

(72) Zettler, F.; Hausen, H. D.; Hess, H. *J. Organomet. Chem.* **1974**, *72*, 157.

(73) Sircoglou, M.; Bontemps, S.; Bouhadir, G.; Saffon, N.; Miqueu, K.; Gu, W.; Mercy, M.; Chen, C.-H.; Foxman, B. M.; Maron, L.; Ozerov, O. V.; Bourissou, D. *J. Am. Chem. Soc.* **2008**, *130*, 16729.

(74) Blagg, R. J.; Charmant, J. P. H.; Connelly, N. G.; Haddow, M. F.; Orpen, A. G. *Chem. Commun.* **2006**, 2350.

(75) Mihalcik, D. J.; White, J. L.; Tanski, J. M.; Zakharov, L. N.; Yap, G. P. A.; Incarvito, C. D.; Rheingold, A. L.; Rabinovich, D. *Dalton Trans.* **2004**, 1626.

(76) Crossley, I. R.; Hill, A. F.; Willis, A. C. *Organometallics* **2006**, *25*, 289.

(77) Goldman, A. S.; Krogh-Jespersen, K. *J. Am. Chem. Soc.* **1996**, *118*, 12159.

(78) Pearson, R. G. *Science* **1966**, *151*, 172.

(79) Burger, B. J.; Bercaw, J. E., Vacuum Line Techniques for Handling Air-Sensitive Organometallic Compounds. In *Experimental Organometallic Chemistry - A Practicum in Synthesis and Characterization*, American Chemical Society: Washington D.C., 1987; Vol. 357, p 79.

(80) Tollefson, M. B.; Li, J. J.; Beak, P. *J. Am. Chem. Soc.* **1996**, *118*, 9052.

(81) Yamashita, M.; Vicario, J. V. C.; Hartwig, J. F. *J. Am. Chem. Soc.* **2003**, *125*, 16347.

(82) Tyburn, J.-M., Bruker Variable Temperature Unit User Manual. In Wissembourg, France, 1998; Vol. 001, p 35.

For Table of Contents Use Only

A Diversity of Metal–Ligand Interactions in Halide (X = I, Br, Cl, F) and Halide-Free Ambiphilic Ligand Rhodium Complexes

Bradley E. Cowie, David J. H. Emslie,* Hilary A. Jenkins,[†] and James F. Britten[†]

TOC Text: A series of ambiphilic ligand rhodium(I) halide complexes, [RhX(CO)(TXPB)] [X = Cl (**1**), Br (**2**), I (**3**) and F (**4**); TXPB = a phosphine/thioether/borane ligand], have been prepared, as well as the halide-free cation [Rh(CO)(TXPB)][PF_6] (**5**). In all complexes, the TXPB ligand binds to rhodium via the phosphine and thioether groups, and in **1** and **2**, bromide and chloride adopt bridging positions between rhodium and boron. By contrast, iodide in **3** binds strongly to rhodium and interacts only weakly with the borane unit in TXPB, while fluoride in **4** binds solely to the borane. In complexes **4** and **5**, approximate square planarity at rhodium is maintained by η^2*CC*-coordination of a *B*–phenyl ring in the anionic TXPB–F ligand, or η^2*BC*-coordination of the borane in TXPB, respectively.

TOC Graphic: